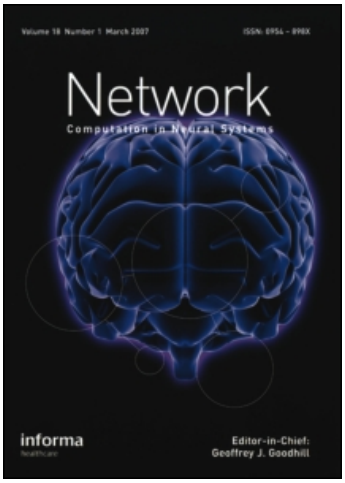

Network: Computation in Neural Systems
Publication details, including instructions for authors and subscription information:
http://www.informaworld.com/smpp/title~content=t713663148

A theory of the influence of eye movements on the refinement of direction selectivity in the cat's primary visual cortex

Antonino Casile [a]; Michele Rucci [b]
[a] Department of Cognitive Neurology, Hertie Institute for Clinical Brain Research, University Clinic, 72076 Tübingen, Germany [b] Departments of Psychology and Biomedical Engineering, and Program in Neuroscience, Boston University, MA

Online publication date: 17 November 2009

To cite this Article Casile, Antonino and Rucci, Michele(2009) 'A theory of the influence of eye movements on the refinement of direction selectivity in the cat's primary visual cortex', Network: Computation in Neural Systems, 20: 4, 197 — 232
To link to this Article: DOI: 10.3109/09548980903314204
URL: http://dx.doi.org/10.3109/09548980903314204

Network: Computation in Neural Systems
December 2009; 20(4): 197–232

informa
healthcare

A theory of the influence of eye movements on the refinement of direction selectivity in the cat's primary visual cortex

ANTONINO CASILE[1] & MICHELE RUCCI[2]

[1]*Department of Cognitive Neurology, Hertie Institute for Clinical Brain Research, University Clinic, 72076 Tübingen, Germany, and* [2]*Departments of Psychology and Biomedical Engineering, and Program in Neuroscience, Boston University, MA 02215*

(Received 16 February 2009; accepted 7 September 2009)

Abstract
Early in life, visual experience influences the refinement of the preferential response for specific stimulus features exhibited by neurons in the primary visual cortex. A striking example of this influence is the reduction in cortical direction selectivity observed in cats reared under high-frequency stroboscopic illumination. Although various mechanisms have been proposed to explain the maturation of individual properties of neuronal responses, a unified account of the joint development of the multiple response features of cortical neurons has remained elusive. In this study, we show that Hebbian synaptic plasticity accounts for the simultaneous refinement of orientation and direction selectivity under both normal and stroboscopic rearing, if one takes into account the spatiotemporal input to the retina during oculomotor activity. In a computational model of the LGN and V1, eye movements are sufficient to establish the patterns of thalamocortical activity required for a Hebbian refinement of both direction- and orientation-selective responses during exposure to natural stimuli. Furthermore, we show that consideration of fixational eye movements explains the simultaneous loss of direction selectivity and preservation of orientation selectivity observed as a consequence of stroboscopic rearing. These results further support a role for oculomotor activity in the refinement of the response properties of V1 neurons.

Keywords: *Visual development, direction selectivity, orientation selectivity, fixational eye movements, primary visual cortex, lateral geniculate nucleus*

Correspondence: Antonino Casile, Hertie Institute for Clinical Brain Research, Department of Cognitive Neurology, Tüingen, Germany. Tel: +49-7071-2987602. Fax: +49-7071-295724. E-mail: antonino.casile@uni-tuebingen.de

ISSN 0954-898X print/ISSN 1361-6536 online/09/040197–232 © 2009 Informa Healthcare Ltd.
DOI: 10.3109/09548980903314204

Introduction

A large percentage of neurons in the primary visual cortex (V1) of the cat respond preferentially to stimuli moving in a specific direction (Hubel and Wiesel, 1959; Hubel and Wiesel, 1962). As for other features of neuronal responses, some degree of directional tuning is already present at the time of eye opening (Hubel and Wiesel, 1963; Pettigrew, 1974; Blakemore and Van Sluyters, 1975), but its full maturation requires normal visual experience (Movshon and Van Sluyters, 1981; Sherman and Spear, 1982; Albus and Wolf, 1984). Indeed, direction-selective responses are markedly reduced in kittens reared in the absence of pattern vision (Pettigrew, 1974; Imbert and Buisseret, 1975; Blakemore and Van Sluyters, 1975) or with abnormal visual input, as in the case of prolonged exposure to high-frequency stroboscopic illumination (Cynader and Chernenko, 1976; Pasternak et al., 1985; Humphrey and Saul, 1998).

Although models have proposed various mechanisms to account for the development of individual properties of the responses of neurons in the primary visual cortex (Bienenstock et al., 1982; Yuille et al., 1989; Moran and Andrade, 1997; Feidler et al., 1997; Wimbauer et al., 1997a; Blais et al., 2000), a unifying explanation of the simultaneous maturation of the many features of cortical responses has remained elusive. This study focuses on the joint refinement, after eye opening, of orientation and direction selectivity. A number of experimental findings (Stryker and Harris, 1986; Fregnac et al., 1988; Chapman and Stryker, 1993; Weliky and Katz, 1997; Miller et al., 1999; Sengpiel and Kind, 2002) support the hypothesis that the development of the spatiotemporal characteristics of V1 neurons relies on a correlation-based mechanism of synaptic plasticity (Stent, 1973; Changeux and Danchin, 1976), which operates initially on spontaneous neural activity and later on visually-driven neuronal responses. Modeling studies have shown the plausibility of this proposal for the emergence of both orientation selectivity (Miyashita and Tanaka, 1992; Miller, 1994) and direction selectivity (Wimbauer et al., 1997a; Wimbauer et al., 1997b) before eye opening. Hebbian plasticity also accounts for the refinement of orientation-selective responses after eye opening (Rucci et al., 2000). However, it remains unclear whether or not Hebbian models provide an explanation for the preservation and refinement of direction selectivity during normal visual experience as well as for its loss during stroboscopic rearing.

Most previous studies have focused on the case of passive exposure to visual stimulation. After eye opening, however, the spatiotemporal stimulus on the retina depends not only on the scene but also on the agent's behavior during the acquisition of visual information. In the cat, as in other species, eye movements are always present under natural viewing conditions, as small saccades and drifts continuously alternate during visual fixation (Ratliff and Riggs, 1950; Ditchburn and Ginsborg, 1953; Steinman et al., 1973; Winterson and Robinson, 1975; Eizenman et al., 1985). The retinal image motion caused by eye movements might contribute to shaping the responses of neurons in the visual system. Experiments in which kittens were raised with their eyes paralyzed have shown basic deficiencies in the development of visually-guided behavior (Hein et al., 1979), as well as impairments in the maturation of ocular dominance and orientation selectivity (Buisseret et al., 1978; Freeman and Bonds, 1979; Singer and Rauschecker, 1982; Gary-Bobo et al., 1986; Buisseret, 1995). Interestingly, cats chronically exposed to stroboscopic light also present peculiar anomalies in the patterns of eye movements (Jones et al., 1981), which may

profoundly influence the structure of neural activity and affect the development of neuronal responses.

We have previously observed that a single correlation-based mechanism of synaptic plasticity is sufficient to explain the development of orientation selectivity before and after eye opening, as fixational eye movements contribute to establishing a regime of neural activity with statistics similar to those of spontaneous activity (Rucci et al., 2000; Rucci and Casile, 2004; Casile and Rucci, 2006). Here, we extend these results to the development of cortical direction selectivity. We show that, in the presence of the physiological motion of the retinal image, a purely Hebbian model also explains the refinement of direction-selective responses during normal visual experience and their loss during stroboscopic rearing. Thus, Hebbian synaptic plasticity provides a powerful theory for describing the maturation of the response characteristics of neurons in the visual system.

Methods

Computational models simulated the visually-evoked responses of neurons in the LGN and V1 of the cat. This section focuses on the elements of the model that are novel to this study. Components of the model described in previous publications are only briefly summarized here (see Rucci and Casile, 2004; Casile and Rucci, 2006).

Modeling neural activity

The model included populations of LGN cells with different spatial and temporal characteristics and V1 simple cells with different degrees of direction selectivity. Neuronal responses to visual stimuli were modeled by means of spatiotemporal filters that replicated the changes in instantaneous firing rate with respect to the level of spontaneous activity. For both geniculate and cortical neurons, responses were generated on the basis of the spatiotemporal convolution between the input image, $I(\boldsymbol{x}, t)$, and the receptive field kernel, $K(\boldsymbol{x}, t)$. That is, the mean instantaneous firing rate at time t of a unit with receptive field centered at position $\boldsymbol{x}$ in the visual field was given by:

$$o(\boldsymbol{x}, t) = \left[K(\boldsymbol{x}, t) \star I(\boldsymbol{x}, t)\right]_\theta = \left[\int_{-\infty}^{\infty}\int_{-\infty}^{\infty}\int_{-\infty}^{\infty} K(\boldsymbol{x}', t')I(\boldsymbol{x} - \boldsymbol{x}' + \boldsymbol{\xi}(t - t'))\mathrm{d}\boldsymbol{x}'\mathrm{d}t'\right]_\theta \tag{1}$$

where $\star$ indicates convolution, $\xi(t) = [\xi_x(t), \xi_y(t)]^T$ represents the eye movement trajectory, and the operator $[\cdot]_\theta$ indicates rectification with threshold θ: $[z]_\theta = z - \theta$ if $z > \theta$, and $[z]_\theta = 0$ if $z \leq \theta$. The results described in this article were collected with a rectification threshold $\theta = 0$ for both geniculate and cortical cells. Highly similar results were obtained for different values of rectification thresholds.

Lateral geniculate nucleus. We simulated the responses of populations of ON- and OFF-center X cells with non-lagged and lagged dynamics. For each unit α, the spatiotemporal kernel $K_\alpha(\boldsymbol{x}, t)$ was modeled as the product of separate spatial (S_α) and temporal (H_α) components:

$$K_\alpha(\boldsymbol{x}, t) = S_\alpha(\boldsymbol{x})H_\alpha(t)$$

Standard difference of Gaussians filters modeled spatial sensitivity:

$$S_\alpha(\boldsymbol{x}) = A_{\text{cnt}} e^{-\frac{\boldsymbol{x}^T\boldsymbol{x}}{2\sigma_{\text{cnt}}^2}} - A_{\text{srn}} e^{-\frac{\boldsymbol{x}^T\boldsymbol{x}}{2\sigma_{\text{srn}}^2}}$$

where A_{cnt}, A_{srn}, σ_{cnt} and σ_{srn} were adjusted on the basis of data from Linsenmeier et al. (1982) to replicate the activity of ON- and OFF-centered cells with receptive fields located at 5° of visual eccentricity.

The impulse responses of non-lagged and lagged geniculate units were modeled as products of polynomial and exponential functions. These functions capture well the biphasic and triphasic profiles observed in LGN neurons (Wimbauer et al., 1997a):

$$\begin{cases} H_\alpha^{\text{NL}}(t) = \frac{1}{W^{\text{NL}}} t(1 - \frac{1}{2}\omega_c t)e^{-\omega_c t} \\ H_\alpha^{\text{L}}(t) = sgn(\omega_s - \omega_c)\frac{1}{W^{\text{L}}}\left\{2\omega_s^2(e^{-\omega_s t} - e^{-\omega_c t}) \right. \\ \qquad \left. + e^{-\omega_c t}\left[t(\omega_s^3 + \omega_c^3 + \omega_s^2\omega_c - 3\omega_c^2\omega_s) - \frac{1}{2}t^2\omega_c(\omega_c + \omega_s)(\omega_s - \omega_c)^2\right]\right\} \end{cases}$$

where the superscripts NL and L indicate non-lagged and lagged units, and W^{NL} and W^{L} are normalizing factors. Parameters were adjusted on the basis of neurophysiological data from Saul et al. (1990). Typical values of the parameters used in the simulations were: $\omega_c = 37.7$ Hz for non-lagged cells and $\omega_c = 25.1$ Hz and $\omega_s = 53.4$ Hz for lagged cells.

V1 simple cells. To ensure that results did not depend on the specific characteristics of simulated V1 units, we modeled five simple cells with different degrees of directional tuning. As shown in Fig. 1(a), for each simulated unit η, we constructed a space-time inseparable kernel, K_η, by linearly combining two separable kernels, K_η^0 and K_η^{90}, whose spatial components differed only for a 90-degree shift in their phases (Adelson and Bergen, 1985; Jagadeesh et al., 1997; DeAngelis et al., 1999):

$$K_\eta(\boldsymbol{x}, t) = K_\eta^0(\boldsymbol{x}, t) + \lambda K_\eta^{90}(\boldsymbol{x}, t) = S_\eta^0(\boldsymbol{x})H_\eta^0(t) + \lambda S_\eta^{90}(\boldsymbol{x})H_\eta^{90}(t) \tag{2}$$

The parameter λ, a scalar ranging from 0 to 1, regulated the degree of inseparability of K_η. A space-time separable receptive field was given by $\lambda = 0$ and a strongly inseparable one by $\lambda = 1$.

The spatial sensitivities of the two separable kernels were modeled by means of Gabor functions:

$$S_\eta(\boldsymbol{x}) = e^{-\frac{1}{2}\boldsymbol{x}^T\Sigma^{-1}\boldsymbol{x}} \cos(2\pi\nu_x x + \phi)$$

where $\Sigma = \begin{pmatrix} \sigma_x^2 & 0 \\ 0 & \sigma_y^2 \end{pmatrix}$ represents the covariance matrix of the Gaussian, and ν_x and ϕ are the spatial frequency and phase of the plane wave, respectively. Spatial parameters were adjusted individually for each cell on the basis of the data reported in Table I in Jones and Palmer (1987). The temporal profiles H_η^0 and H_η^{90} were identical to those of non-lagged and lagged cells (H_α^{NL} and H_α^{L}, respectively) as neurons in the LGN and V1 tend to possess similar temporal dynamics (Saul and Humphrey, 1992; Alonso et al., 2001).

The response characteristics of V1 receptive fields were quantified by means of indices. The degree of orientation selectivity was measured as in Liao et al. (2004) on the basis of the change in response to a grating with preferred orientation and

optimal spatial and temporal frequencies (R_p) relative to the response obtained with the same grating rotated by 45° (R_{45}). These responses were combined into an Orientation Selectivity Index: $OSI = 1 - \frac{R_{45}}{R_p}$, ranging from 0 to 1.

The degree of direction selectivity was quantified by means of a Direction Selectivity Index (DSI), which weighted the response difference to gratings with optimal spatial and temporal frequencies moving in the preferred (R_p) and non-preferred directions (R_{np}): $DSI = \frac{R_p - R_{np}}{R_p + R_{np}}$ (DeAngelis et al., 1993). This index ranged from 0 to 1, with 1 indicating no response for the non-preferred direction of motion.

Visual Stimulation

Stimuli. Visual input to the model was provided by 15 pictures of natural scenes selected from a public domain database (van Hateren and Ruderman, 1998). The size of these images was 1536×1024 pixels, corresponding to a visual area of approximately $25° \times 17°$ degrees. The radial mean of the power spectrum of this selected pool of images was best interpolated by $S(f) \approx f^{-1.95}$. The similarity between this estimate and the power spectra measured on larger databases indicates that the selected set of images well represented the statistical characteristics of natural scenes (Field, 1987).

A trial in our simulations consisted in the presentation of one of the images of the database for a period of 6 s. An initial fixation point was randomly selected on the image at the beginning of each trial. Starting from this initial point, the direction of gaze moved to model different types of eye movements. In simulations of normal rearing, visual input was continually presented to the model throughout the duration of the trial. In simulations of 8-Hz stroboscopic rearing, visual input was flashed for a single time step of the stimulation (1 ms) every 125 ms. Neurophysiological recordings in the cat have shown that neuronal responses to brief, high-intensity flashes are significantly longer than the durations predicted by linear models. This effect has been observed both at the level of the retina (see Fig. 1 in Levick and Zacks (1970); Kratz and May, 1990) and in the primary visual cortex (Duysens et al., 1985). In order to replicate this nonlinear phenomenon by means of the quasi-linear filters of our neuronal models, we incorporated the extended sensitivity to the stimulus into the visual input itself, by prolonging the stimulus in the intervals between the flashes with exponential decay. This persistence of the stimulus is not meant to imply the presence of light in the interval between successive stroboscopic flashes. It is only a convenient way to model the non-linear impact of stroboscopic illumination on cell responses.

Eye movements. During presentation of an image, the receptive fields of model neurons moved in a way that replicated the natural alternation of saccades and periods of fixational movements. Saccades were modeled by a generalized exponential distribution of fixation times, which produced an average of roughly 2 saccades/s (Harris et al., 1988). Each saccade possessed random amplitude and direction, which were selected so as to keep fixation within the image. Saccadic amplitude replicated the bimodal distribution observed in the cat. More specifically, the amplitudes of smaller saccades (<70′) were uniformly distributed around their mean of 35′, whereas the amplitudes of larger saccades followed a

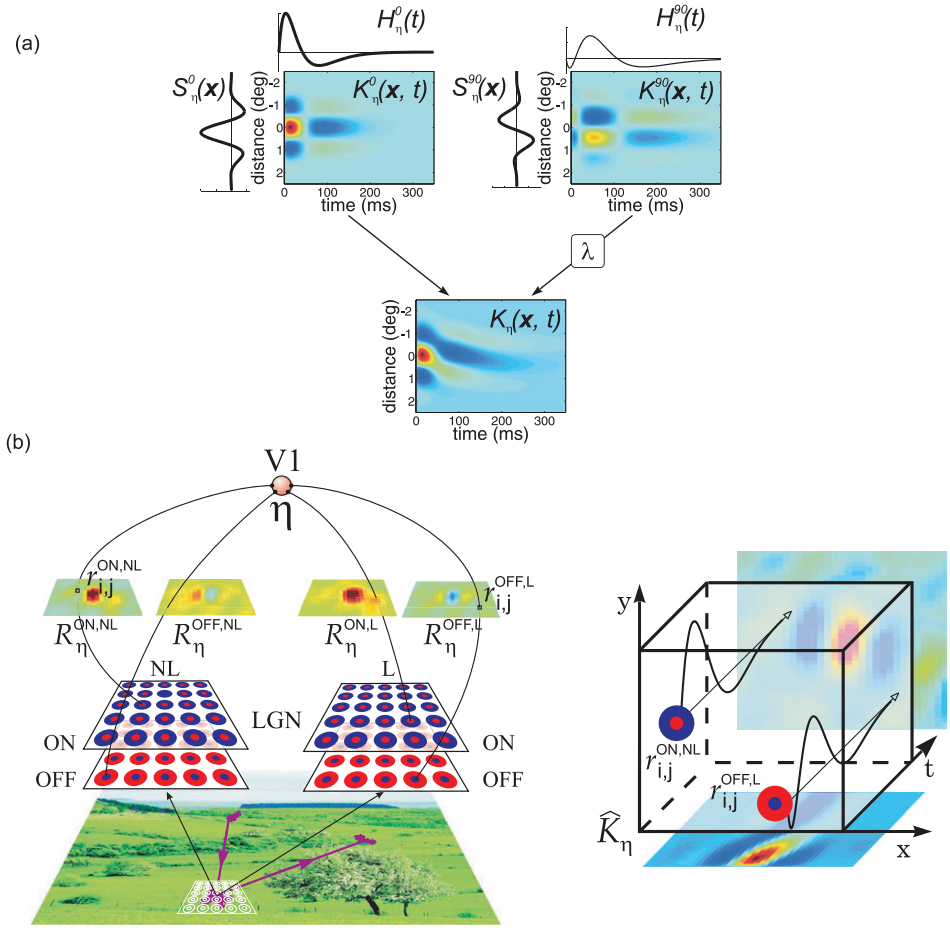

Figure 1. Modeling approach. (a) Model of a V1 simple cell. The visually-evoked responses of V1 neurons were simulated by means of the sum of two space-time separable filters: $K^0_\eta(\boldsymbol{x}, t)$ and $K^{90}_\eta(\boldsymbol{x}, t)$ (see Eq. 2). (b) Procedure for estimating the impact of neural activity on Hebbian development. (*Left*) For each modeled V1 simple cell, η, levels of correlation were measured with the responses of four arrays of LGN units while sequences of simulated eye movements scanned images of natural scenes. Each array contained units with the same polarity p (ON- or OFF-center) and the same temporal dynamics d (non-lagged or lagged) and yielded a corresponding pattern of correlation $\mathcal{R}^{p,d}_\eta(\boldsymbol{x})$. The value $r^{p,d}_{i,j}$ in each pattern represents the level of correlation between η and the LGN unit at location i, j in the array. (*Right*) The spatiotemporal kernel resulting from the structure of correlated activity, $\widehat{K}_\eta(\boldsymbol{x}, t)$ (the *correlation kernel*), was estimated as the linear combination of input contributions from all geniculate units, each geniculate input weighted by the unit's average level of correlation r with η. This kernel was used to predict the direction of the developmental trajectory, *i.e.*, whether the statistics of input stimulation would lead to a loss or enable preservation of the initial degree of selectivity exhibited by a V1 neuron. Note that a correlation kernel does not represent a prediction of the cell receptive field at the end of the critical period. The results of simulations in which synaptic changes were explicitly modeled are reported in Appendix B.

Gaussian distribution with a mean of 5.3° and a standard deviation of 3.17° (Winterson and Robinson, 1975). Saccadic directions were uniformly distributed. The duration of a saccade was proportional to its amplitude as described in the literature (Ditchburn, 1973). Fixational drift and tremor were modeled together by means of a two-dimensional stochastic stationary process. This process possessed Gaussian second-order statistics with temporal and spatial standard deviations of 10 ms and 10′, respectively. As shown in the *Results* section, the specific values of these parameters had little influence on the results of the simulations.

In order to accurately replicate the eye movements observed in cats reared under stroboscopic light (Jones et al., 1981), a sinusoidal oscillation was superimposed onto a slow and smooth drift. The oscillation amplitude was 0.75°, which is the average amplitude of strobe-induced nystagmus measured experimentally (Jones et al., 1981). Drift was modeled by means of a Gaussian stationary process with temporal and spatial standard deviations of 100 ms and 3′, respectively. This model yielded excellent fits of published traces of eye movements recorded from kittens reared under stroboscopic illumination (Jones et al., 1981).

Analysis of thalamocortical activity

The goal of this study is to determine whether the stimuli present on the retina under various rearing conditions would lead to a loss or enable preservation of the initial degree of selectivity exhibited by V1 neurons at the time of eye opening. In the presence of purely Hebbian synapses, the direction of the developmental trajectory can be predicted directly from the structure of thalamocortical activity at the opening of the period of plasticity. Thus, in the main simulations of this study, we examined the patterns of correlation in the responses of cortical and geniculate neurons without implementing synaptic modifications. The results of simulations in which synaptic changes were explicitly modeled are reported in Appendix B.

For each modeled V1 neuron η, we measured the correlation with the responses of arrays of geniculate cells with different spatial (ON- or OFF-center) and temporal (non-lagged or lagged) characteristics. As illustrated in Fig. 1(b), LGN units were arranged into four 21×21 arrays (one array for each geniculate population) aligned with the Y-axis parallel to the preferred orientation of the cortical neuron. The receptive fields of geniculate units were evenly spaced to cover the entire receptive field of η. The strength of the correlation between a geniculate and the cortical unit was given by the temporal average of the product of their activities.

Levels of correlation measured in the simulations were then used to compute the kernel $\widehat{K}_\eta(\boldsymbol{x}, t)$ resulting from the structure of thalamocortical activity (for convenience, the "*correlation kernel*" of cell η). This kernel was evaluated by summing up the spatiotemporal receptive fields of all the 1764 geniculate units in the model, each weighted by a factor proportional to the correlation between the considered LGN unit and the V1 unit η:

$$\widehat{K}_\eta(\boldsymbol{x}, t) = \sum_{i,j} r_{i,j}^{\mathrm{ON,NL}} K_{i,j}^{\mathrm{ON,NL}}(\boldsymbol{x}, t) + r_{i,j}^{\mathrm{ON,L}} K_{i,j}^{\mathrm{ON,L}}(\boldsymbol{x}, t) + r_{i,j}^{\mathrm{OFF,NL}} K_{i,j}^{\mathrm{OFF,NL}}(\boldsymbol{x}, t) + r_{i,j}^{\mathrm{OFF,L}} K_{i,j}^{\mathrm{OFF,L}}(\boldsymbol{x}, t) \tag{3}$$

where $K_{i,j}^{p,d}$ represents the 3-D kernel of the geniculate unit at position (i, j) in the array of cells with polarity p (ON- or OFF-centered) and timing d (non-lagged or lagged), and $r_{i,j}^{p,d}$ is the strength of the correlation between this geniculate unit and the cortical neuron η.

Comparison of the correlation kernel, $\widehat{K}_\eta$, and η's spatiotemporal receptive field, K_η, determines in which direction the response characteristics of η will evolve during visual experience. A V1 neuron will certainly preserve, and possibly refine, its orientation and direction selectivity, if the spatiotemporal tuning of the correlation kernel is similar to, or higher than, the tuning exhibited by the cell at the time of eye opening. The initial degree of response tuning will instead be eventually lost, if the correlation kernel is less selective than the cell. In the simulations presented in this paper, levels of correlation were averaged over a total of 3000 trials, *i.e.*, 200 trials for each of the 15 images in the database. The 2D spatial and spatiotemporal sections of receptive fields showed in the following sections were obtained by slicing the 3D kernels at time $t = 40$ ms and along the axis perpendicular to the cell's preferred orientation, respectively.

Results

The visually-evoked responses of geniculate and cortical neurons were modeled by means of independent spatiotemporal filters, which were designed on the basis of published neurophysiological data. As explained in the *Methods*, the model consisted of 1764 LGN neurons and five V1 simple cells. The LGN model included ON- and OFF-center, non-lagged and lagged, X neurons at equally-spaced position in the visual field. Models of V1 cells were designed as the sum of two space-time separable elements with different timings to possess different degrees of direction and orientation selectivity. The mean Direction Selectivity Index (DSI) across modeled V1 units was 0.55 ± 0.08, which is approximately equal to the average value measured in kittens (Saul and Feidler, 2002). The mean Orientation Selectivity Index (OSI) was 0.85 ± 0.18.

In order to determine whether a neuron would lose or preserve its orientation and direction selectivity during visual experience, we compared the receptive field of each modeled cell to the corresponding kernel resulting from the patterns of correlated activity (the *correlation kernel*, see Fig. 1(b)). With a purely Hebbian scheme of synaptic plasticity, analysis of the correlation kernel is sufficient to predict the direction of the developmental trajectory. The following two sections analyze the structure of thalamocortical activity in simulations of normal and stroboscopic rearing. Appendix B reports the results of simulations that explicitly modeled synaptic modifications.

Normal Rearing

To study the impact of normal visual experience on the refinement of the response characteristics of V1 neurons, we simulated neural activity when images of natural scenes were scanned by sequences of eye movements that replicated the oculomotor behavior of normally-reared cats. Figure 2 summarizes the results of these simulations.

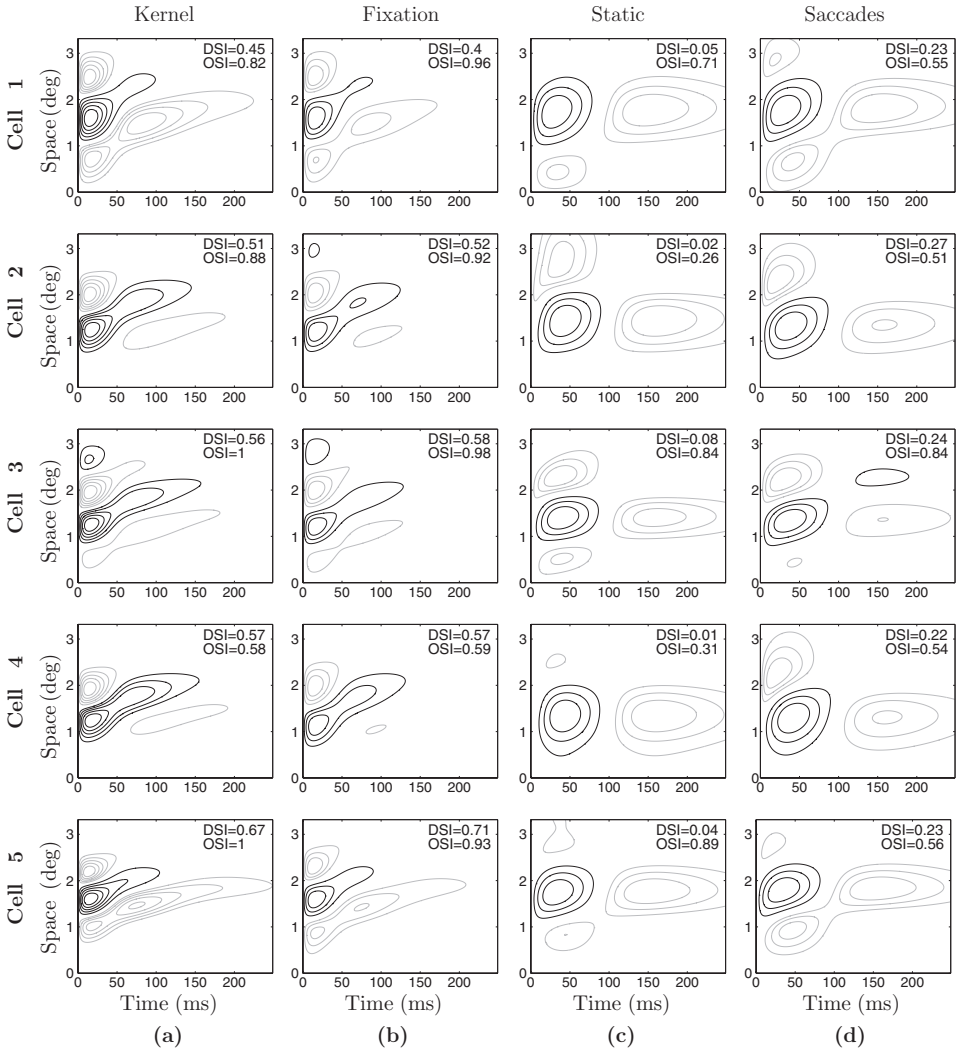

Figure 2. Influences of eye movements on the refinement of the receptive fields of V1 neurons. Results for five simulated simple cells are shown on separate rows. Column (a) shows spatiotemporal sections of the kernels of modeled units. (*Kernel*). Columns (b–d) show the kernels given by the structure of thalamocortical activity (the "*correlation kernels*") measured in the following viewing conditions: during sustained fixation, when only fixational eye movements occurred (*Fixation*); during static presentation of visual stimulation (*Static*); and during sequences of eye movements that included only non-fixational saccades (*Saccades*). Sections were obtained by slicing the 3D kernels along the plane perpendicular to the cell's preferred orientation. Black and gray lines in the kernels represent ON and OFF subregions, respectively. The values of the corresponding indices of orientation and direction selectivity are shown in each panel.

For each of the five modeled simple cells, the panels in Fig. 2 (b–d) show the kernels given by the structure of correlated activity during different oculomotor regimes. Fig. 2 (b) illustrates the correlation kernels measured during sustained fixation. In these simulations, visual fixation was maintained for the entire duration

of a trial (6 s), and only fixational eye movements occurred during this period. It is clear from these data that correlation kernels measured under these conditions were very similar to the actual spatiotemporal kernels of neuronal models (mean DSI: 0.55 ± 0.11; mean OSI: 0.88 ± 0.16). During development, this similarity would result in a smooth developmental transition between the periods pre- and post-eye opening, as it implies that the patterns of correlation occurring immediately after eye opening would match the pattern of connectivity established by the cortical cell before eye opening. Thus, during the normal instability of visual fixation, a Hebbian stabilization of thalamocortical afferents would continue strengthening pre-existing directional and orientation biases in the responses of V1 neurons, even though the statistics of external visual stimulation are very different from those of endogenous spontaneous activity.

The results of Fig. 2(b) contrast with those obtained in the absence of retinal image motion. The receptive fields of model cells did not move in the simulations of Fig. 2(c). A fixation point was randomly selected for each of the 3000 trials over which averages were calculated, and visual input to the model did not change during the entire duration of the trial. As shown by the panels in Fig. 2(c), correlation kernels measured in the absence of retinal image motion contained abnormally large ON and OFF subregions and were separable in their spatial and temporal components. These kernels exhibited virtually no direction selectivity (mean DSI: 0.04 ± 0.03) and a substantial reduction in orientation selectivity with respect to model neurons (mean OSI $= 0.60 \pm 0.30$). In the presence of Hebbian synapses, this pattern of correlated activity would act to lower the degree of spatiotemporal tuning exhibited by V1 neurons at the time of eye opening.

While these data show that motion of the retinal image is necessary for the normal maturation of V1 receptive fields, not every type of retinal image motion has an effect similar to that of fixational instability. Fig. 2(d) shows the patterns of correlated activity measured when oculomotor activity only consisted of normal (non-fixational) saccades. These patterns were very similar to those obtained with static presentation of retinal input (mean DSI $= 0.24 \pm 0.02$; mean OSI $= 0.60 \pm 0.13$). Thus, the retinal image motion resulting from fixational eye movements appeared to be necessary to give rise to a regime of thalamocortical activity consistent with the normal refinement of direction and orientation selectivity.

To further examine the influence of fixational eye movements on neural activity, Fig. 3 shows levels of correlation between the responses of one simulated cortical neuron (Cell 1 in Fig. 2) and the responses of a selected subset of LGN units. The receptive fields of these selected geniculate units were equally spaced to compose a line array orthogonal to the preferred orientation of the simple cell. This line intersected the receptive field of the simple cell at its center. The data in Fig. 3 show two important points. First, they clarify that the spatiotemporal inseparability of the correlation kernel originated from the spatial segregation of non-lagged and lagged geniculate units in the patterns of correlated activity. That is, during fixational eye movements, the response of the simple cell was maximally correlated with the responses of non-lagged and lagged units at different locations. In the correlation kernel, this spatial segregation in inputs with different dynamics yields a gradient in the timing of the response elicited by stimulation of different regions of the kernel. Note that such segregation of thalamic inputs

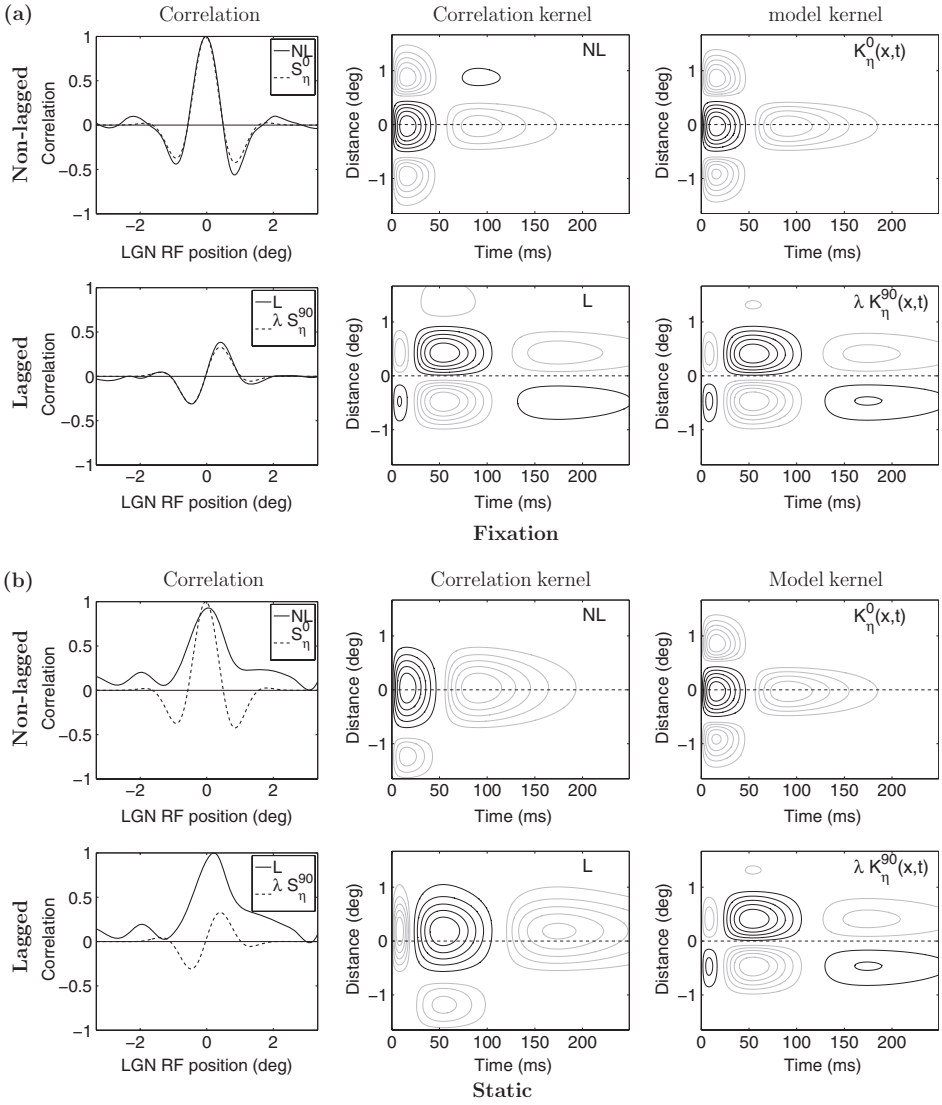

Figure 3. Structure of correlated activity for one cortical unit (Cell 1 in Fig. 2) in simulations of normal rearing. Results obtained during sustained fixation (*Fixation*) and during static exposure to visual stimulation (*Static*) are shown in (a) and (b), respectively. In both viewing conditions, panels are organized as follows: (*Left column*) Levels of correlation between the response of Cell 1 and those of line-arrays of non-lagged (*NL*, *top*) and lagged (*L*, *bottom*) LGN units. The receptive fields of geniculate neurons were centered at evenly-spaced locations on a line orthogonal to the preferred orientation of the V1 cell. This line cut in half the receptive field of the V1 neuron. At each spatial location on the *x* axis, levels of correlation with OFF-center units were subtracted from those with ON-center units. Thus, positive values in the curves indicate locations at which the V1 unit established stronger correlation with ON- rather than OFF-center LGN units. The opposite occurs for negative values. The spatial organizations of the two space-time separable components of Cell 1's receptive field (S_η^0 and λS_η^{90} in Eq. 2) are also shown for comparison. (*Center column*) Contributions to the correlation kernel of Cell 1 from geniculate units with non-lagged (*NL*, *top*) and lagged dynamics (*L*, *bottom*). (*Right column*) Spatiotemporal sections of the two space-time separable components of Cell 1's kernel (the terms $K_\eta^0(\boldsymbol{x}, t)$ and $\lambda K_\eta^{90}(\boldsymbol{x}, t)$ in Eq. 2).

did not occur during static exposure to visual stimulation, when the simple cell was strongly correlated with non-lagged and lagged geniculate units at the same location (see Fig. 3(b)). This pattern of correlated activity yields a space-time separable kernel that is not direction selective.

The second important point shown by the data in Fig. 3 is that the two patterns of correlated activity established by the V1 unit with populations of non-lagged and lagged geniculate units resembled, both in their spatial arrangements and relative strengths, the two spatial elements composing the cell kernel (S_η^0 and λS_η^{90} in Eq. 2). Because of this similarity, the contribution to the correlation kernel from geniculate units closely matched the two components of the cortical receptive field (K_η^0 and λK_η^{90} in Eq. 2). More specifically, the contribution from non-lagged geniculate units closely matched K_η^0, whereas the contribution from lagged units matched λK_η^{90} (see central and right columns in Fig. 3(a)). Since these two components are summed up to evaluate the correlation kernel, the resulting kernel's organization was highly similar to that of the receptive field of the modeled unit. Again, this similarity did not occur during static exposure to visual stimulation, when input contributions from non-lagged and lagged geniculate units did not match the spatial arrangements of K_η^0 and λK_η^{90} (Fig. 3(b)).

To understand the origins of the similarity between modeled receptive fields and correlation kernels, we derived analytical estimates of the structure of correlated activity (see Appendix A). Closed-form approximations of the patterns of thalamo-cortical correlated activity can be obtained by eliminating the operation of rectification in the generation of neuronal responses. In the absence of rectification, models acted purely as linear filters. Thus, the correlation between the responses of cortical and geniculate units can be calculated directly in the frequency domain on the basis of the response characteristics of model units and the power spectrum of the retinal stimulus.

The analysis summarized in Appendix A relies on an approximation of the spatiotemporal stimulus on the retina during fixational eye movements. We observed that during fixation, the visual input experienced at time t by a receptor at location $\boldsymbol{x}$ on the retina, $I_r(\boldsymbol{x}, t)$, can be decomposed as the sum of two input signals: a constant signal $I_r(\boldsymbol{x}, 0)$ given by the initial value of the luminance impinging on retinal position $\boldsymbol{x}$ during the fixation period, and the signal $\widetilde{I}_r(\boldsymbol{x}, t)$ given by the deviation at time t from this value. Under the assumption of fixational eye movements with small amplitude, the fixational modulations of luminance, $\widetilde{I}_r$, can be approximated by means of a Taylor series on the basis of the spatial derivatives of the stimulus (Casile and Rucci, 2006). As explained in Appendix A, this approximation yields the following estimate of the power spectrum of $\widetilde{I}_r$:

$$P_{\widetilde{I}\widetilde{I}}(\boldsymbol{f}, u) \approx |\boldsymbol{f}|^2 P_S(\boldsymbol{f}) R_{\xi\xi}(u) \tag{4}$$

where $\boldsymbol{f}$ and u represent, respectively, spatial and temporal frequencies, P_S is the spectrum of the stimulus, and $R_{\xi\xi}$ is the spectrum of fixational eye movements.

Equation 4 shows that the power spectrum of the fixational modulations of luminance is approximately space-time separable. In the temporal domain, the statistics of these fluctuations are determined by the characteristics of eye movements (the term $R_{\xi\xi}$). In the spatial domain, this input signal is given by the power spectrum of the stimulus multiplied by the square of spatial frequency. As described in Appendix A, analytical estimates obtained on the basis of Eq. 4 gave

excellent fits of the structure of correlated activity measured in simulations of the full model, showing that the results of our simulations were primarily due to the impact of fixational modulations of luminance.

The mathematical analysis of Appendix A demonstrates that the matching between patterns of correlated activity and receptive fields shown in Figs. 2 and 3 originated from fundamental statistical properties of the retinal stimulus during fixational eye movements. Both the temporal and spatial statistics of fixational modulations of luminance played an important role.

In the temporal domain, the characteristics of eye movements were instrumental to ensuring that geniculate neurons with different timings would form independent patterns of correlated activity. During fixational instability, the correlation between the responses of a V1 cell, η, and a geniculate neuron, α, was only dependent on the space-time separable component in η's kernel that possessed the same timing of α. Correlations with the other kernel's component were negligible. That is, levels of correlation with non-lagged neurons were only a function of $S_\eta^0(\boldsymbol{x})$, whereas only $S_\eta^{90}(\boldsymbol{x})$ influenced levels of correlation with lagged units. This separation occurred because the temporal profiles of non-lagged and lagged geniculate neurons were approximately orthogonal under the metric given by fixational eye movements. As described below, this effect does not occur with non-fixational eye movements.

In the spatial domain, fixational eye movements caused modulations of luminance to be uncorrelated during viewing of natural images. Unlike other categories of images, natural scenes are characterized by a very specific spectral distribution; their power spectrum declines proportionally to the square of the spatial frequency (Field, 1987). Thus, during viewing of natural images, P_S and $|\boldsymbol{f}|^2$ counterbalanced each other in Eq. 4, yielding an almost flat spectral distribution. A broad power spectrum corresponds to a narrow correlation in the spatial domain. As a consequence of this "*whitening*", levels of correlation in our simulations were only determined by the spatial convolution of cell receptive fields, as during stimulation with spatial white noise. With the typical spatial characteristics of geniculate cells and V1 neurons, this convolution is very similar to the considered V1 kernel (Casile and Rucci, 2006).

In summary, our theoretical analysis shows that the similarity between V1 receptive fields and correlation kernels originated from the combination of two factors, both of them determined by the spatiotemporal characteristics of the retinal stimulus. First, because of the temporal structure of eye movements, the responses of geniculate cells with different timings were uncorrelated. Thus, the response contribution of each of the two space-time separable components in the model of a V1 cell was strongly correlated only with the responses of LGN units with the same timing. Secondly, each of these two patterns of correlation matched the spatial organization of the corresponding space-time separable component. This matching occurred because of the lack of spatial correlations in the fixational modulations of luminance present during viewing of natural images.

Furthermore, since our analysis does not rely on the specific structure of S_η^0 and S_η^{90}, Appendix A also shows that the results obtained for the five neurons in the simulations of Figs. 2 and 3 extend to all V1 neurons whose response characteristics can be modeled by means of Eq. 2, a model that captures the wide diversity of simple cell responses in V1 (Jones and Palmer, 1987; DeAngelis et al., 1999).

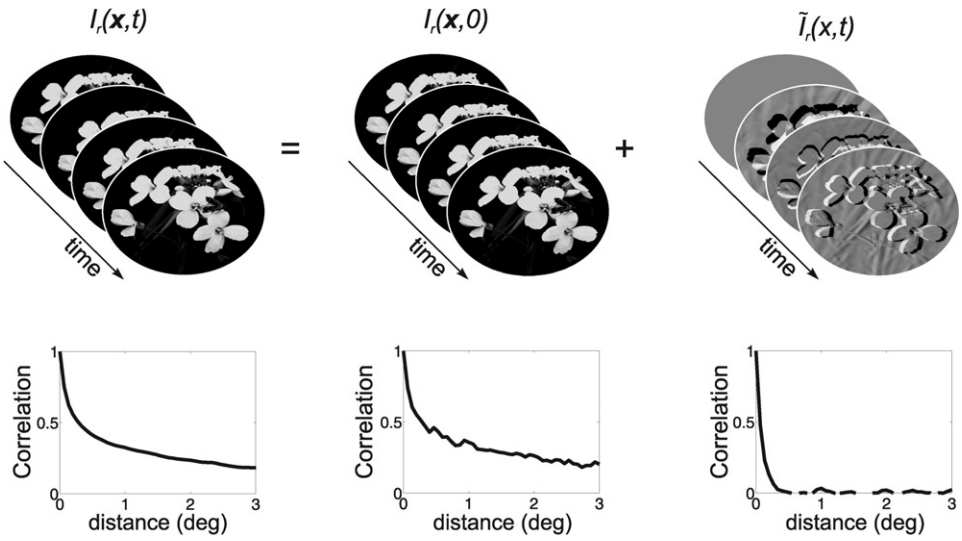

Figure 4. An approximation of the retinal stimulus during fixational instability. At each instant in time t, the input signal $I_r(\boldsymbol{x}, t)$ impinging on the retina can be split into the sum of two images: a static image $I_r(\boldsymbol{x}, 0)$ representing the input at time $t = 0$ at retinal location $\boldsymbol{x}$, and a time-varying image $\tilde{I}_r(\boldsymbol{x}, t)$, in which each pixel represents the instantaneous deviation of visual input with respect to $I_r(\boldsymbol{x}, 0)$: $I_r(\boldsymbol{x}, t) = I_r(\boldsymbol{x}, 0) + \tilde{I}_r(\boldsymbol{x}, t)$. Equation 4 gives an approximation of the power spectrum of $\tilde{I}_r$. Each graph in the bottom row shows the average correlation in pixel intensity in the individual frames of the movie above. Spatial correlations are narrower in $\tilde{I}_r(\boldsymbol{x}, t)$ than in the original stimulus.

For these neurons, correlation kernels will always be highly similar to receptive fields when natural images are observed through jittering eyes.

Correlation kernels did not match modeled receptive fields when the spatio-temporal stimulus on the retina did not possess the characteristics described above. Figure 5 compares the mean DSI and OSI of the five modeled V1 neurons to those of the correlation kernels measured under various viewing conditions. Both direction and orientation selectivity were lost when same natural images used in the simulations of Fig. 2 were examined in the presence of large-amplitude nystagmus. In these simulations, normal fixational instability was replaced by 8-Hz sinusoidal nystagmus with a peak-to-peak amplitude of 4°. The luminance modulations caused by this behavior were abnormal in both their spatial and temporal statistics. This signal did not yield an orthogonalization of responses from geniculate units with different timings nor spatial whitening. As a consequence, both orientation and direction selectivity were markedly reduced in the correlation kernels (mean DSI $= 0.29 \pm 0.07$; mean OSI $= 0.51 \pm 0.1$).

In contrast, Fig. 5 shows that only orientation selectivity was attenuated when fixational eye movements scanned stimuli with statistics different from those of natural images (mean DSI $= 0.62 \pm 0.2$, mean OSI $= 0.54 \pm 0.17$). In these simulations, model neurons were exposed to visual input with power spectrum that declined as $|\boldsymbol{f}|^{-6}$ instead of the normal $|\boldsymbol{f}|^{-2}$. Direction selectivity was preserved under these conditions, because the presence of normal fixational eye movements enabled segregated contributions from geniculate neurons with different timings.

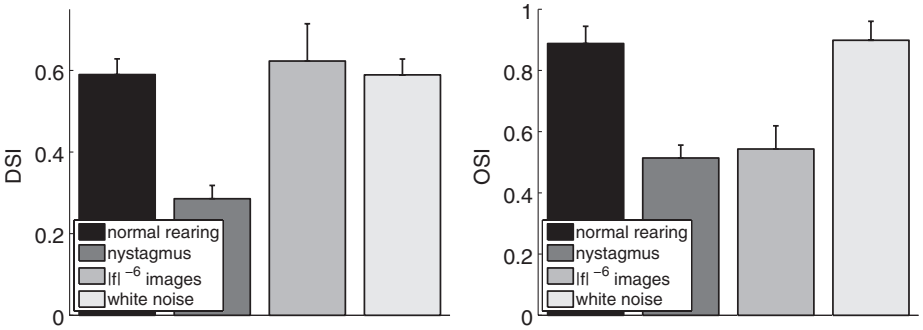

Figure 5. Characteristics of correlation kernels measured under various viewing conditions. The mean DSI and OSI of correlation kernels in simulations of normal rearing are compared to the corresponding values obtained: during viewing of natural images with large-amplitude nystagmus (*nystagmus*); during viewing of images with $|\boldsymbol{f}|^{-6}$ spectrum and normal fixational instability ($|\boldsymbol{f}|^{-6}$ *images*); and during presentation of spatial white noise (*white noise*). Data represent means ± s.e. over the set of 5 simulated units.

This segregation continued to yield a spatial gradient of response timings. However, fixational modulations contained spatial correlations, as the spectral density $|\boldsymbol{f}|^2$ $P_S(\boldsymbol{f})$ in Eq. 4 was no longer flat with $|\boldsymbol{f}|^{-6}$ images. These input correlations led to an enlargement of the ON and OFF subregions of correlation kernels, therefore attenuating orientation selectivity.

As shown by the data in Fig. 5, the results of our simulations of normal rearing were very similar to those obtained during fixation on white noise stimuli (normal rearing: mean DSI $= 0.59 \pm 0.09$, mean OSI $= 0.89 \pm 0.13$; white noise: mean DSI $= 0.59 \pm 0.09$, mean OSI $= 0.90 \pm 0.14$). These images do not contain spatial correlations and the effect of the $|\boldsymbol{f}|^2$ term in Eq. 4 was negligible. Thus, our model makes the prediction that the maturation of orientation and direction selectivity does not require exposure to a visual environment that contains edges or objects. Visual exposure to white noise patterns during the critical period should be sufficient for a normal refinement of orientation and direction selectivity.

Figure 6 examines the degree of robustness of our results with respect to systematic variations in the main parameters of the model. Figure 6(a) illustrates the impact of the degree of spatiotemporal inseparability of modeled neurons. This feature is controlled by the parameter λ in Eq. 2. For each modeled V1 cell, we systematically varied the value of λ and measured the degree of direction selectivity in the resulting correlation kernel. Data points in Fig. 6(a) represent the mean DSI of correlation kernels for the five modeled neurons. Correlation kernels possessed a slightly higher DSI than modeled receptive fields. Thus, when natural images are viewed through the normal instability of visual fixation, even V1 units with low directional biases would preserve and refine their directional preference in the presence of a Hebbian mechanism of synaptic plasticity.

Figure 6(b) shows the effect of altering the characteristics of fixational eye movements. To this end, the spatial and temporal variances of the fixational motion of the retinal image (the term $\mathcal{R}_{\xi\xi}(u)$ in Eq. 4) were parametrically varied. Higher values of spatial and temporal variances yielded, respectively, larger and smoother fixational eye movements. Data in Fig. 6(b) represent the average DSI of correlation

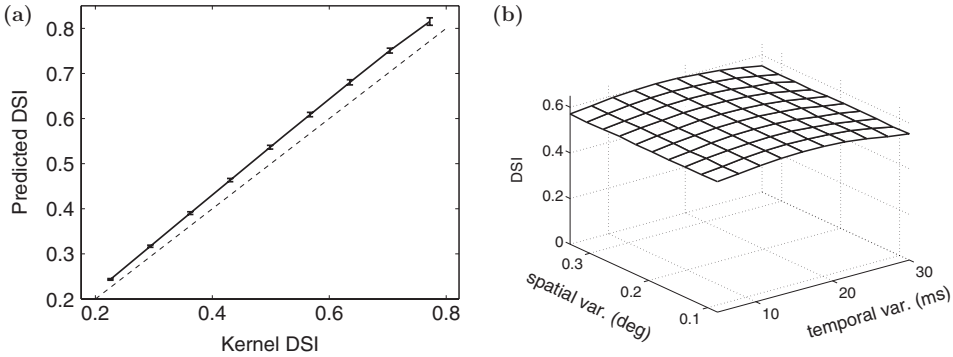

Figure 6. Robustness of results of normal rearing with respect to changes in model parameters. (a) Effect of varying the degree of space-time inseparability of modeled cortical units (parameter λ in Eq. 2). The mean DSI of correlation kernels is plotted as a function of the mean DSI of modeled neurons. Vertical bars represent standard errors over the 5 simulated units. (b) Effect of altering the statistics of fixational eye movements. Data points represent the mean DSI obtained in the presence of eye movements with varying degrees of amplitude and smoothness.

kernels over the five simulated V1 units. The little variability of the resulting surface implies that similar values of direction selectivity were obtained in the presence of retinal image motion with different characteristics around its normal structure. That is, while abnormal oculomotor activity significantly influenced simulation results, correlation patterns were insensitive to the fine characteristics of fixational eye movements.

Stroboscopic Rearing

Chronic exposure to stroboscopic illumination is known to drastically impair the maturation of direction selectivity. Neurons in the striate cortex of kittens reared under stroboscopic light with relatively high frequency (8 Hz) lack direction selectivity, while they appear normal with respect to other features of their responses including selectivity for the stimulus' orientation (Cynader and Chernenko, 1976; Pasternak et al., 1985). The reasons underlying this specific loss of directional preference are not known. Interestingly, kittens reared under 8-Hz stroboscopic illumination also exhibit abnormal oculomotor activity. Whereas saccades appear normal, visual fixations are characterized by pronounced nystagmus with main frequency equal to the frequency of the strobe light (Jones et al., 1981). We used our model to investigate whether the statistics of visual input experienced by these cats might provide an explanation for the developmental effects of stroboscopic rearing.

Figure 7 shows the results of simulations of stroboscopic rearing. Visual input in these simulations was given by the same set of natural images already used in the case of normal rearing. However, in order to model the retinal stimulus experienced by cats chronically exposed to stroboscopic illumination, the input image was flashed every 125 ms for one time step of the simulation (1 ms), while simulated

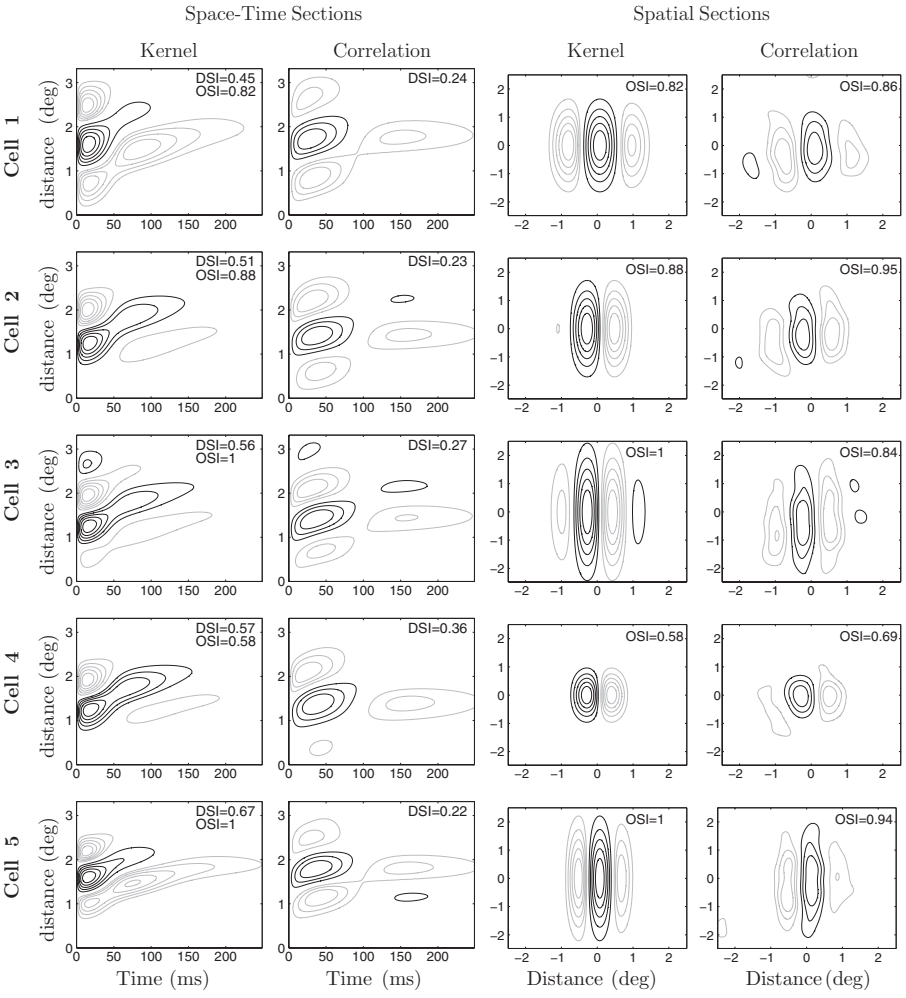

Figure 7. Correlation kernels measured in simulations of stroboscopic rearing. Visual input to the model replicated the retinal stimulus experienced by cats reared under 8-Hz stroboscopic illumination. Results for five simulated V1 units are shown on separate rows. Sections of modeled receptive fields (*Kernel*) are compared to equivalent sections of the correlations kernels (*Correlation*). Both spatiotemporal (*left*) and spatial (*right*) sections are shown. Spatiotemporal sections were obtained by slicing the 3D kernels at time $t = 40$ ms. Highly similar results were obtained for different values of t.

eye movements replicated the oculomotor behavior observed in strobe-reared cats (see *Methods*). The columns of Fig. 7 compare the receptive fields of the five simple cells already studied in the case of normal visual experience to the kernels given by the structure of thalamocortical activity. Levels of correlation were measured during visual fixation, as in the simulations of Fig. 2(b). The data in Fig. 7 show that the structure of neural activity measured under these conditions yielded correlation kernels that were spatially oriented but lacked spatiotemporal inseparability. This spatiotemporal structure gives selectivity for the orientation of the stimulus but not for its direction of motion. The average indices of orientation and direction selectivity of the correlation kernel measured for the 5 simulated V1 units were

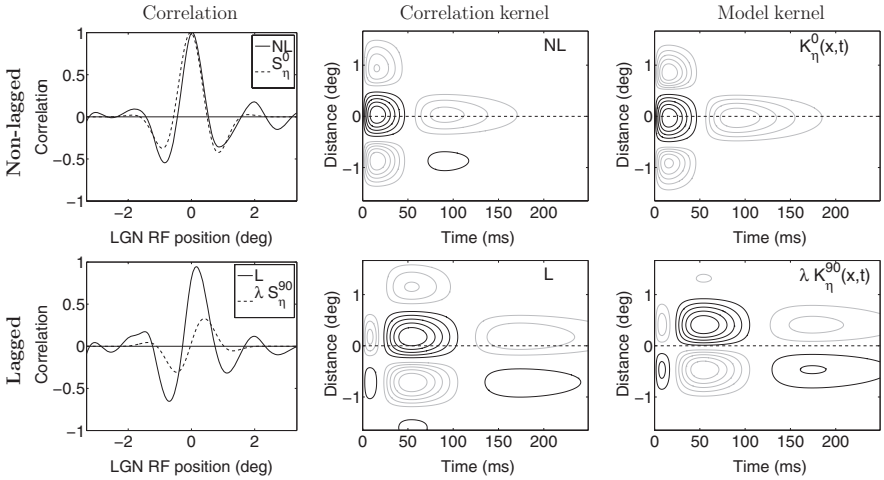

Figure 8. Structure of correlated activity for one cortical unit (Cell 1 in Fig. 2) in simulations of stroboscopic rearing. The layout of the panels is the same as in Fig. 3. (*Left column*) Levels of correlation between the response of Cell 1 and those of line-arrays of non-lagged (*NL*, *top*) and lagged (*L*, *bottom*) LGN units, respectively. At each spatial location on the *x* axis, levels of correlation with OFF-center units were subtracted from those with ON-center units, so that positive (negative) values indicate that the V1 unit was more (less) strongly correlated with ON- rather than OFF-center LGN units. The spatial organizations of the two space-time separable components of Cell 1's receptive field (S_η^0 and S_η^{90} in Eq. 2) are shown for comparison. (*Center column*) Contributions to the correlation kernel of Cell 1 from geniculate units with non-lagged (*NL*, *top*) and lagged dynamics (*L*, *bottom*). (*Right column*) Spatiotemporal sections of the two space-time separable components of Cell 1's kernel (the terms $K_\eta^0(\boldsymbol{x}, t)$ and $\lambda K_\eta^{90}(\boldsymbol{x}, t)$ in Eq. 2).

0.86 ± 0.1 and 0.27 ± 0.06, respectively. These results are consistent with the characteristics of neuronal responses measured in the striate cortex of cats reared under stroboscopic illumination (Cynader and Chernenko, 1976; Humphrey and Saul, 1998).

Figure 8 shows levels of correlation between the responses of a cortical unit (Cell 1) and the responses of line arrays of LGN units. As in Fig. 3, these arrays crossed the receptive field of the simple cell at its center and were aligned orthogonally to the cell's preferred orientation. The structure of correlated activity observed in these simulations was profoundly different from that measured in simulations of normal rearing. Unlike the case of normal rearing, the two patterns of correlation formed by geniculate populations of non-lagged and lagged units resembled each other during stroboscopic rearing. That is, whereas in simulations of normal rearing the contributions to the correlation kernel from non-lagged and lagged LGN neurons matched the two space-time separable components in the model of the considered simple cell (K_η^0 and λK_η^{90} in Eq. 2), this spatial segregation did not occur during stroboscopic rearing. Instead, inputs from geniculate cells with different timings blended together in simulations of stroboscopic rearing, and each region of the simple cell's correlation kernel received input contributions from both non-lagged and lagged units.

While the two populations of geniculate units with different dynamics established similar patterns of correlated activity, within each population, levels of correlation

exhibited by neurons with different polarities remained spatially segregated. The curves in the top panels of Fig. 8 represent differences in the correlated activity of geniculate units with different polarity. Cell 1′s levels of correlation with OFF-center units were subtracted from those with ON-center units at the same spatial location, so that positive and negative values indicate that Cell 1 was more strongly correlated with ON- and OFF-center LGN units, respectively. As shown by these data, Cell 1 established strong correlations with ON- and OFF-center geniculate units located in different subregions of its receptive field. These pools of correlated geniculate units with the same polarity formed spatially elongated subregions in the correlation kernel. It was the simultaneous occurrence of (a) a spatial segregation of inputs from geniculate units with different polarities, and (b) a lack of segregation of inputs from geniculate units with different timings, which was responsible for the formation of correlation kernels that possessed good orientation selectivity and poor direction selectivity.

In order to understand the factors responsible for the results of our simulations, we followed an approach similar to that of the previous section and derived analytical approximations of the second-order statistics of thalamocortical activity in a simplified linear version of the model. This analysis, summarized in Appendix A, is an extension of the analysis conducted in the case of normal rearing. It shows that, as with the simulations of normal rearing, also the results of the simulations of stroboscopic rearing can be predicted on the basis of the way the stimulus on the retina changes with time. Unlike normal rearing, however, dynamic fluctuations of luminance experienced under stroboscopic illumination depend not only on oculomotor activity, but also on the temporal arrangement of the stroboscopic flashes.

As explained in Appendix A, the stimulus on the retina during stroboscopic illumination can again be decomposed into the sum of two separate static and time-varying signals in a similar way to Fig. 4. Under the assumption of small displacements of the direction of gaze at the time of occurrence of the flashes, the input changes of luminance $\widetilde{I}_r(\boldsymbol{x}, t)$ can still be approximated on the basis of the spatial derivatives of the stimulus, an approximation which yields a space-time separable estimate of the power spectrum:

$$P_{\widetilde{I}\widetilde{I}}(\boldsymbol{f}, u) \approx |\boldsymbol{f}|^2 P_S(\boldsymbol{f}) Q(u) \tag{5}$$

where P_S is the power spectrum of the external stimulus, and the temporal spectral density Q depends on both the frequency content of eye movements and the train of flashes.

In the spatial domain, Eq. 5 shows that the characteristics of retinal stimulation during normal and stroboscopic rearing are highly similar. The term $|\boldsymbol{f}|^2$ in Eq. 5 counterbalances the frequency proportionality exhibited by P_S during viewing of natural images, yielding a spatially uncorrelated input signal. This lack of spatial correlation as responsible for the segregation of the responses of ON- and OFF-center neurons into separate elongated regions in the patterns of correlated activity and for the resulting orientation tuning of correlation kernels.

In the temporal domain, the retinal stimuli present during normal and stroboscopic rearing differed significantly. Whereas the temporal fluctuations of luminance were entirely dependent on the characteristics of eye movements during normal rearing (the term $R_{\xi\xi}(u)$ in Eq. 4), they were also affected by the flashes

during stroboscopic rearing (the term $Q(u)$ in Eq. 5). The main consequence of these flashes was to alter the way geniculate responses correlated with the responses of cortical units. Contrary to the case of normal rearing, the temporal profiles of non-lagged and lagged units were not orthogonal under the metric provided by $Q(u)$. That is, a geniculate unit with a given timing (non-lagged or lagged) was no longer only correlated with the component with the same timing within the response of the cortical unit, but established strong correlations with both components. Therefore, the contributions to correlation kernels from non-lagged and lagged geniculate units did ot match $K_\eta^0(\boldsymbol{x}, t)$ and $\lambda K_\eta^{90}(\boldsymbol{x}, t)$ as in the simulations of normal rearing. Non-lagged and lagged contributions were instead highly similar to each other, both approximately equal to the sum of $K_\eta^0(\boldsymbol{x}, t)$ and $K_\eta^{90}(\boldsymbol{x}, t)$. Thus, correlation kernels exhibited similar response timings at all spatial locations, a pattern that would lead to the loss of direction selectivity during development.

The mathematical analysis of Appendix A makes clear that the characteristics of eye movements maintain a profound influence on thalamocortical activity under conditions of stroboscopic illumination. This effect is somewhat counterintuitive, as stroboscopic illumination seems to freeze retinal image motion. Figure 9 shows the impact of various types of eye movements. The degree of direction selectivity of correlation kernels dropped by more than a factor of 2, when images of natural scenes were examined in the presence of nystagmus synchronized with the stroboscopic flashes, the oculomotor activity exhibited by cats reared under stroboscopic illumination (mean DSI normal rearing: 0.59 ± 0.09. Mean DSI stroboscopic rearing $= 0.26 \pm 0.01$). This result is in agreement with the observation that the majority of simple cells possess a DSI lower than 0.3 in cats reared under stroboscopic illumination (see Fig. 2 B in Humphrey and Saul, 1998). Orientation selectivity was instead minimally affected by this change in viewing conditions (mean OSI normal rearing $= 0.89 \pm 0.13$. Mean OSI stroboscopic rearing: 0.87 ± 0.16).

In the previous simulations, the input to the model replicated the nystagmus observed in kittens chronically exposed to stroboscopic illumination.

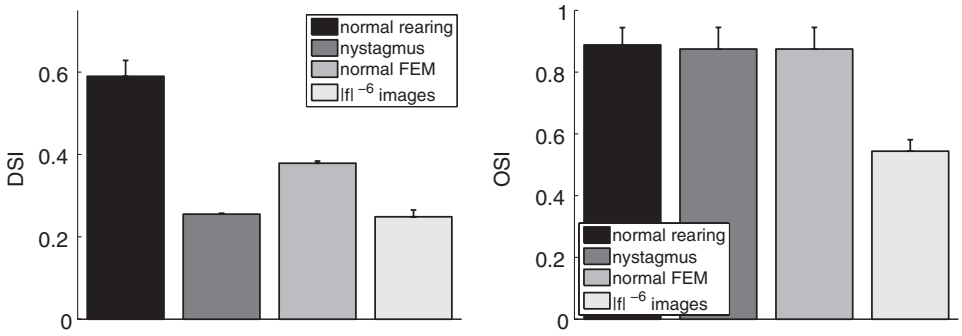

Figure 9. Characteristics of correlation kernels measured under various conditions of stroboscopic rearing. The mean DSI and OSI measured during normal rearing are compared to those obtained in the presence of stroboscopic flashes and (1) small-amplitude nystagmus (*nystagmus*); (2) normal fixational eye movements (*normal FEM*); (3) visual input with $|\boldsymbol{f}|^{-6}$ spectral density and nystagmus ($|\boldsymbol{f}|^{-6}$ *images*). Data represent means ± s.e. over the set of 5 simulated units.

However, nystagmus presumably develops gradually during visual experience. To better examine the developmental impact of abnormal oculomotor activity, we also run simulations of stroboscopic rearing in which nystagmus was substituted by normal fixational eye movements. As shown by the data in Fig. 9, exposure to stroboscopic illumination gave rise to correlation kernels with a very low degree of direction selectivity (mean DSI $= 0.38 \pm 0.01$) and high orientation selectivity (mean OSI $= 0.87 \pm 0.16$) independent of the precise characteristics of fixational instability. Interestingly, even though nystagmus was not the main cause for the poor direction selectivity of correlation kernels, its presence yielded values of DSI closer to those measured in neurophysiological experiments. This result suggests that abnormal fixational eye movements might contribute to the loss of cortical direction selectivity observed in kittens reared under stroboscopic light.

As in the simulations of normal rearing, manipulation of the spatial structure of the stimulus significantly affected the degree of orientation selectivity in patterns of correlated activity. Fig. 9 shows results obtained with presentation of visual input with $|\boldsymbol{f}|^{-6}$ power spectrum. These stimuli were scanned by the same nystagmus used in the previous simulations. The ON and OFF subregions of correlation kernels were larger under these conditions than with presentation of natural stimuli. This effect, in conjunction with the temporal impact of stroboscopic flashes, led to correlation kernels with poor degrees of both orientation and direction selectivity (mean DSI $= 0.25 \pm 0.04$; mean OSI $= 0.54 \pm 0.08$).

Figure 10 examines the robustness of our results. The degree of direction selectivity of correlation kernels was minimally influenced by the strength of the directional bias exhibited by V1 neurons at the time of eye opening. The DSI of patterns of correlation never exceeded 0.25 irrespective of the degree of directional tuning of modeled receptive fields (Fig. 10(a)). Thus, according to our model, even neurons sharply tuned for a specific direction of motion will eventually lose their selectivity during prolonged exposure to stroboscopic illumination.

Figure 10(b) examines the impact of the characteristics of nystagmus. Data points represent the mean DSI of the correlation kernels measured during nystagmus with

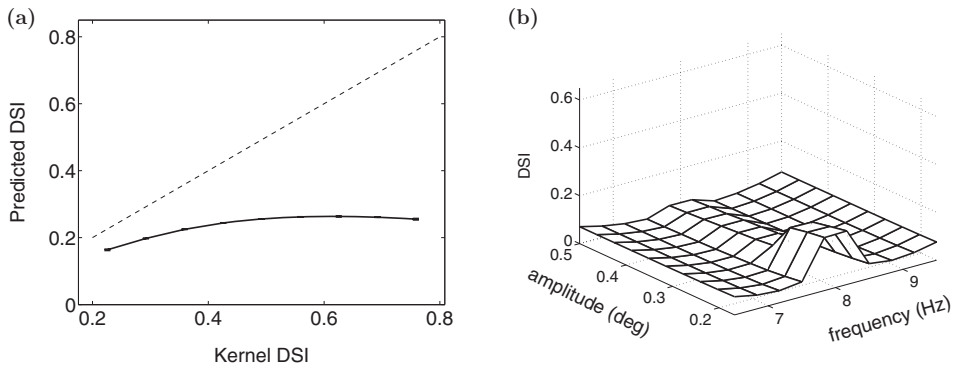

Figure 10. Robustness of the results of stroboscopic rearing. (a) Impact of the degree of space-time inseparability of modeled cortical units (the parameter λ in Eq. 2). The mean DSI of correlation kernels is plotted as a function of the mean DSI of simulated receptive fields. Error bars represent s.e. (b) Impact of the characteristics of nystagmus. Data points represent the mean DSI measured with nystagmus with different amplitudes and frequencies.

various amplitudes and frequencies. In these simulations, the drift component of the model of eye movements was left unchanged, while we varied the parameters of the sinusoidal oscillation. These data, together with the results of Fig. 9 show that correlation kernels were little sensitive to the fine structure of fixational eye movements. Direction selectivity varied slightly with the frequency of nystagmus, exhibiting a peak at 8 Hz, but always remaining significantly lower than the values measured in simulations of normal rearing. Thus, the poor direction selectivity of the patterns of correlated activity measured during stroboscopic illumination was a robust result, minimally affected by the precise characteristics of our model.

Discussion

Under natural viewing conditions, observers are not passively exposed to the incoming flow of sensory data. Rather, they actively relocate their gaze in order to seek useful information. The results of this study show that input modulations caused by eye movements are sufficient to (a) establish a regime of neural activity compatible with a Hebbian maturation of direction-selective V1 cells, and (b) account for the simultaneous loss of directional preference and preservation of orientation selectivity observed in cats reared under stroboscopic illumination. These results originate from the statistical properties of input signals to the retina during oculomotor activity and are unaffected by the fine characteristics of neuronal models.

A substantial body of evidence indicates that the physiological instability of fixation is an important component of the way visual information is acquired and encoded in the brain. Microscopic eye movements are always present during natural fixation and translate the retinal image across many receptors (Ratliff and Riggs, 1950; Yarbus, 1967; Steinman et al., 1973; Ditchburn, 1980; see Martinez-Conde et al. (2004) for a review). Psychophysical studies that eliminated retinal image motion—a procedure known as retinal stabilization—have shown that images tend to fade (Ditchburn and Ginsborg, 1952; Riggs and Ratliff, 1952; Yarbus, 1967) and that the processing of fine spatial detail is impaired when the stimulus remains immobile on the retina (Rucci et al., 2007). Modulations exerted by fixational eye movements in the responses of retinal ganglion cells seem to facilitate feature estimation (Greschner et al., 2002) and figure-ground segregation (Olveczky et al., 2003). Furthermore, fixational eye movements strongly modulate neuronal responses in the striate cortex and LGN of macaques (Gur et al., 1997; Leopold and Logothetis, 1998; Martinez-Conde et al., 2000; Martinez-Conde et al., 2002; Snodderly et al., 2001). All these findings support the proposal that the fixational motion of the retinal image influences activity-dependent processes of synaptic modifications in the developing visual system.

In previous modeling studies, we suggested that fixational eye movements contribute to establishing a regime of neural activity compatible with the maturation of distinct ON and OFF subregions in the receptive fields of simple cells (Rucci et al., 2000; Rucci and Casile, 2004; Casile and Rucci, 2006). The results of the present study extend this hypothesis to LGN neurons with different response timings. In simulations of normal rearing, the average pattern of geniculate activity consisted of spatially-segregated ensembles of coactive units with different dynamics (non-lagged and lagged) and polarities (ON- and OFF-center). This dual

segregation was the consequence of the spatiotemporal characteristics of fixational modulations of luminance. Fixational modulations were uncorrelated in space because of the statistics of natural images, and their temporal structure was such that neurons with different timings possessed uncorrelated responses. In the presence of Hebbian synapses, the pattern of correlated activity measured in our simulations would lead to the maturation of V1 neurons that are selective for both the direction and orientation of the stimulus.

In contrast, in simulations of stroboscopic rearing, the presence of the flashes led to strong correlations between geniculate units with different timings. Fixational modulations of luminance were still spatially uncorrelated, but their temporal structure did not enable a segregation of the responses of units with different dynamics, as in the case of normal rearing. Thus, only units with different polarities formed distinct coactive pools in the simulations of stroboscopic rearing. These ensembles included units with both non-lagged and lagged dynamics. Consistent with experimental findings, this structure of neural activity would lead to the development of simple cells with orientation-selective responses but little or no direction selectivity.

Like most previous developmental models of direction selectivity (Feidler et al., 1997; Wimbauer et al., 1997b; Blais et al., 2000), this study has focused on the refinement of thalamic inputs to V1 cells. Several experimental observations indicate that the precise organization of geniculate afferents is an important component of neuronal preference for a specific direction of motion. Indeed, it has been shown that the timings of responses elicited from stimulation of different regions within the receptive field of a simple cell closely resemble those of non-lagged and lagged neurons (Saul and Humphrey, 1992). Furthermore, the response dynamics of geniculate and direction-selective V1 neurons tend to evolve in a similar way during development (Saul and Feidler, 2002). Direction-selective responses are also preserved during cooling the cortex, a procedure that attenuates intracortical interactions and emphasizes thalamic influences (Ferster et al., 1996). Thus, the temporal diversity of geniculate responses appear to provide a first directional bias, which is then refined by intra-cortical mechanisms (Suarez et al., 1995; Maex and Orban, 1996; Crook et al., 1998; Murthy and Humphrey, 1999).

While the focus on cortical input is common to most previous theoretical analysis of the development of direction selectivity, there are important aspects that differentiate our model from previous ones. A first critical difference is our focus on the refinement of direction selectivity during visual experience, rather than on its initial emergence. In the cat, direction-selective responses emerge before eye opening (Pettigrew, 1974; Braastad and Heggelund, 1985; Albus and Wolf, 1984). According to our model, visual experience contributes to the maturation of direction selectivity by refining receptive fields that already possess a directional bias. These initial biases could originate from a number of sources and, in fact, are to be expected given the implausibility of a perfectly isotropic structure in the developing patterns of neuronal connectivity. Independent of its origin, even a slight initial preference for a direction of motion will be preserved and strengthened during active exposure to natural visual stimulation. In this view, the modest increase during the critical period in the total number of direction selective neurons reported by Albus and Wolf (1984) may originate from including in the later

count cells that possessed a bias that was too weak to be reliably detected at the time of eye opening.

A further significant distinction with respect to previous models is our examination of the impact of oculomotor activity. Whereas previous models used arbitrarily generated motion signals, this is the first study to explicitly examine the influences of eye movements on the maturation of direction selectivity. In our model, fixational instability was necessary for establishing a regime of thalamo-cortical activity compatible with the Hebbian refinement of space-time inseparable receptive fields. Visual experience without eye movements led to the loss of both direction and orientation selectivity.

Following an approach similar to that of our previous modeling studies (Rucci et al., 2000; Rucci and Casile, 2005; Casile and Rucci, 2006), the developmental consequences of chronic exposure to different types of retinal stimulation were inferred from the structure of correlated activity in the model. This approach is justified by the observation that purely Hebbian synapses change their strengths proportionally to the degree of correlation in the responses of their pre- and postsynaptic elements. Thus, with this scheme of synaptic plasticity, levels of correlation at the time of eye opening are sufficient to determine the direction in which development will evolve. More specifically, a V1 cell will preserve, and possibly continue strengthening its initial selectivity, if the pattern of correlated activity established with geniculate units has a similar organization to, or is more sharply tuned than, the cell's receptive field at the time of eye opening. In contrast, the same V1 neuron will instead become less selective during visual experience, if the structure of correlation yields a less sharply tuned response than the initial response exhibited by the neuron. Correlations kernels in our study were used solely to make this prediction, not to estimate the actual structure of a cell's receptive field at the end of the critical period. Additional simulations, in which synaptic connectivity and Hebbian changes were modeled explicitly, have confirmed the validity of this approach (see Appendix B).

The results of this study lead to a number of well-defined experimental predictions. The main prediction is that exposure to visual stimulation *per se* is not sufficient for the maturation of direction selectivity, but that visual experience should occur in the presence of eye movements. Eye movements have already been shown to be critical during visual development (Hein et al., 1979). More specifically, impairments in the plasticity underlying both ocular dominance (Freeman and Bonds, 1979; Singer and Rauschecker, 1982) and orientation selectivity (Buisseret, 1995) have been observed in kittens exposed to visual experience with their eyes paralyzed. While a few hours of normal visual experience within a critical period are sufficient to reestablish orientation-selective responses in dark-reared kittens, elimination of eye movements during exposure to light prevents such restoration (Buisseret et al., 1978; Gary-Bobo et al., 1986). Furthermore, it has been reported that a normal reestablishment of orientation selectivity occurs in the presence of eye movements, even if other movements of the body are selectively prevented (Buisseret and Gary-Bobo, 1979). Experiments aimed at specifically analyzing the developmental influences of fixational eye movements have not been conducted.

Another interesting prediction of this study is that a normal maturation of direction selectivity should also take place in kittens reared in static environments,

in which egomotion is the only source of retinal image motion. The patterns of correlation described in this article occur for any small jitter of the retinal image irrespective of its origin, *i.e.*, whether resulting from behavior or from the actual motion of the stimulus. For example, the trembling of leaves on a tree with the wind would yield in our model patterns of thalamocortical correlated activity similar to those measured in the presence of fixational eye movements. Yet, given that eye movements are always present, the retinal image motion resulting from oculomotor activity should be sufficient for the normal refinement of direction selectivity. Furthermore, according to this theory, the refinement of direction selectivity does not even require the presence of smooth retinal motion, as it may intuitively appear to be necessary. In our simulations, a normal refinement of cortical direction selectivity also occurred in the presence of fixational eye movements with very low degree of smoothness (see Fig. 6(b)).

A further prediction made by our model regards the specific patterns of thalamocortical connectivity that emerge during stroboscopic rearing. Humphrey et al. (1998) reported that, in the striate cortex of strobe-reared cats, different regions within the receptive field of a V1 neuron exhibit similar response timings. On the basis of this observation, these authors proposed that stroboscopic rearing might prevent the convergence of inputs with different response timings onto simple cells. Our model instead predicts that geniculate cells with different temporal characteristics project onto the same cortical neuron also under conditions of stroboscopic rearing. However, since, these projections originate from nearby cells, their contributions blend together at each location within the receptive fields of a V1 neuron, and these inputs cannot be easily distinguished.

Studies analyzing the role of visual experience on cortical development often focus on the characteristics of the scene without taking into account the observer's behavior. Yet, egomotion is a fundamental contributor to the statistics of the spatiotemporal stimulus on the retina. This study argues that a trace of the existence of the fixational motion of the retinal image can be found in some of the most basic properties of neuronal responses, such as orientation and direction selectivity. Furthermore, our results raise the hypothesis that the abnormal fixational eye movements observed in various pathological conditions (Martinez-Conde, 2006) might contribute to the development of the visual impairments associated with these disorders. Further studies are needed to investigate this hypothesis and examine whether other features of neuronal responses are similarly affected by oculomotor activity.

Acknowledgments

This work was supported by the DFG grant SFB550-C10, NIH grant 5R01EY18363, NSF grants BCS-0719849 and CCF-0726901 and the Hermann and Lilly Schilling Foundation.

References

Adelson EH, Bergen JR. 1985. Spatiotemporal energy models for the perception of motion. J Opt Soc Am A 2:284–99.

Albus K, Wolf W. 1984. Early post-natal development of neuronal function in the kitten's visual cortex: A laminar analysis. J Physiol 348:153–85.

Alonso JM, Usrey WM, Reid RC. 2001. Rules of connectivity between geniculate cells and simple cells in cat primary visual cortex. J Neurosci 21:4002–15.

Bienenstock EL, Cooper LN, Munro PW. 1982. Theory for the development of neuron selectivity: Orientation specificity and binocular interaction in visual cortex. J Neurosci 2:32–48.

Blais B, Cooper LN, Shouval H. 2000. Formation of direction selectivity in natural scene environments. Neural Comput 12:1057–66.

Blakemore C, Van Sluyters RC. 1975. Innate and environmental factors in the development of the kitten's visual cortex. J Physiol 248:663–716.

Braastad BO, Heggelund P. 1985. Development of spatial receptive-field organization and orientation selectivity in kitten striate cortex. J Neurophysiol 53:1158–78.

Buisseret P. 1995. Influence of extraocular muscle proprioception on vision. Physiol Rev 75:323–38.

Buisseret P, Gary-Bobo E. 1979. Development of visual cortical orientation specificity after dark-rearing: Role of extraocular proprioception. Neurosci Lett 13:259–63.

Buisseret P, Gary-Bobo E, Imbert M. 1978. Ocular motility and recovery of orientational properties of visual cortical neurones in dark-reared kittens. Nature 272:816–7.

Casile A, Rucci M. 2006. A theoretical analysis of the influence of fixational instability on the development of thalamocortical connectivity. Neural Comput 18:569–90.

Changeux JP, Danchin A. 1976. Selective stabilisation of developing synapses as a mechanism for the specification of neuronal networks. Nature 264:705–12.

Chapman B, Stryker MP. 1993. Development of orientation selectivity in ferret visual cortex and effects of deprivation. J Neurosci 13:5251–62.

Crook JM, Kisvrday ZF, Eysel UT. 1998. Evidence for a contribution of lateral inhibition to orientation tuning and direction selectivity in cat visual cortex: Reversible inactivation of functionally characterized sites combined with neuroanatomical tracing techniques. Eur J Neurosci 10:2056–75.

Cynader M, Chernenko G. 1976. Abolition of direction selectivity in the visual cortex of the cat. Science 193:504–5.

DeAngelis GC, Ghose GM, Ohzawa I, Freeman RD. 1999. Functional micro-organization of primary visual cortex: Receptive field analysis of nearby neurons. J Neurosci 19:4046–64.

DeAngelis GC, Ohzawa I, Freeman RD. 1993. Spatiotemporal organization of simple-cell receptive fields in the cat's striate cortex. I. General characteristics and postnatal development. J Neurophysiol 69:1091–117.

Ditchburn RW. 1973. Eye-Movements and Visual Perception : Oxford University Press.

Ditchburn RW. 1980. The function of small saccades. Vision Res 20:271–2.

Ditchburn RW, Ginsborg BL. 1952. Vision with a stabilized retinal image. Nature 170:36–7.

Ditchburn RW, Ginsborg BL. 1953. Involuntary eye movements during fixation. J Physiol 119:1–17.

Duysens J, Orban GA, Cremieux J, Maes H. 1985. Visual cortical correlates of visible persistence. Vision Res 25:171–8.

Eizenman M, Hallett PE, Frecker RC. 1985. Power spectra for ocular drift and tremor. Vision Res 25:1635–40.

Feidler JC, Saul AB, Murthy A, Humphrey AL. 1997. Hebbian learning and the development of direction selectivity: The role of geniculate response timings. Network 8:195–214.

Ferster D, Chung S, Wheat H. 1996. Orientation selectivity of thalamic input to simple cells of cat visual cortex. Nature 380:249–52.

Field DJ. 1987. Relations between the statistics of natural images and the response properties of cortical cells. J Opt Soc Am A 4:2379–94.

Freeman RD, Bonds AB. 1979. Cortical plasticity in monocularly deprived immobilized kittens depends on eye movement. Science 206:1093–5.

Fregnac Y, Shulz D, Thorpe S, Bienenstock E. 1988. A cellular analogue of visual cortical plasticity. Nature 333:367–70.

Gary-Bobo E, Milleret C, Buisseret P. 1986. Role of eye movements in developmental processes of orientation selectivity in the kitten visual cortex. Vision Res 26:557–67.

Greschner M, Bongard M, Rujan P, Ammermüller J. 2002. Retinal ganglion cell synchronization by fixational eye movements improves feature estimation. Nat Neurosci 5:341–7.

Gur M, Beylin A, Snodderly DM. 1997. Response variability of neurons in primary visual cortex (V1) of alert monkeys. J Neurosci 17:2914–20.

Harris CM, Hainline L, Abramov I, Lemerise E, Camenzuli C. 1988. The distribution of fixation durations in infants and naive adults. Vision Res 28:419–32.

Hein A, Vital-Durand F, Salinger W, Diamond R. 1979. Eye movements initiate visual-motor development in the cat. Science 204:1321–2.

Hubel DH, Wiesel TN. 1959. Receptive fields of single neurones in the cat's striate cortex. J Physiol 148:574–91.

Hubel DH, Wiesel TN. 1962. Receptive fields, binocular interaction and functional architecture in the cat's visual cortex. J Physiol 160:106–54.

Hubel DH, Wiesel TN. 1963. Receptive fields of cells in striate cortex of very young, visually inexperienced kittens. J Neurophysiol 26:994–1002.

Humphrey AL, Saul AB. 1998. Strobe rearing reduces direction selectivity in area 17 by altering spatiotemporal receptive-field structure. J Neurophysiol 80:2991–3004.

Humphrey AL, Saul AB, Feidler JC. 1998. Strobe rearing prevents the convergence of inputs with different response timings onto area 17 simple cells. J Neurophysiol 80:3005–20.

Imbert M, Buisseret P. 1975. Receptive field characteristics and plastic properties of visual cortical cells in kittens reared with or without visual experience. Exp Brain Res 22:25–36.

Jagadeesh B, Wheat HS, Kontsevich LL, Tyler CW, Ferster D. 1997. Direction selectivity of synaptic potentials in simple cells of the cat visual cortex. J Neurophysiol 78:2772–89.

Jones G, Mandl G, Cynader M, Outerbridge JS. 1981. Eye oscillations in strobe reared cats. Brain Res 209:47–60.

Jones JP, Palmer LA. 1987. An evaluation of the two-dimensional gabor filter model of simple receptive fields in cat striate cortex. J Neurophysiol 58:1233–58.

Kratz KE, May JG. 1990. Response persistence of cat retinal ganglion cells to the temporally discrete presentation of sinewave gratings. Int J Neurosci 52:111–9.

Leopold DA, Logothetis NK. 1998. Microsaccades differentially modulate neural activity in the striate and extrastriate visual cortex. Exp Brain Res 123:341–5.

Levick WR, Zacks JL. 1970. Responses of cat retinal ganglion cells to brief flashes of light. J Physiol 206:677–700.

Liao DS, Krahe TE, Prusky GT, Medina AE, Ramoa AS. 2004. Recovery of cortical binocularity and orientation selectivity after the critical period for ocular dominance plasticity. J Neurophysiol 92:2113–21.

Linsenmeier RA, Frishman LJ, Jakiela HG, Enroth-Cugell C. 1982. Receptive field properties of X and Y cells in the cat retina derived from contrast sensitivity measurements. Vision Res 22:1173–83.

Maex R, Orban GA. 1996. Model circuit of spiking neurons generating directional selectivity in simple cells. J Neurophysiol 75:1515–45.

Martinez-Conde S. 2006. Fixational eye movements in normal and pathological vision. Prog Brain Res 154:151–76.

Martinez-Conde S, Macknik SL, Hubel DH. 2000. Microsaccadic eye movements and firing of single cells in the striate cortex of macaque monkeys. Nat Neurosci 3:251–8.

Martinez-Conde S, Macknik SL, Hubel DH. 2002. The function of bursts of spikes during visual fixation in the awake primate lateral geniculate nucleus and primary visual cortex. Proc Natl Acad Sci USA 99:13920–5.

Martinez-Conde S, Macknik SL, Hubel DH. 2004. The role of fixational eye movements in visual perception. Nat Rev Neurosci 5:229–40.

Miller KD. 1994. A model for the development of simple cell receptive fields and the ordered arrangement of orientation columns through activity-dependent competition between ON- and OFF-center inputs. J Neurosci 14:409–41.

Miller KD, Erwin E, Kayser A. 1999. Is the development of orientation selectivity instructed by activity? J Neurobiol 41:44–57.

Miyashita M, Tanaka S. 1992. A mathematical model for the self-organization of orientation columns in visual cortex. Neuroreport 3:69–72.

Moran F, Andrade MA. 1997. Receptive field map development by anti-Hebbian learning. Neural Netw 10:1037–1052.

Movshon JA, Van Sluyters RC. 1981. Visual neural development. Annu Rev Psychol 32:477–522.

Murthy A, Humphrey AL. 1999. Inhibitory contributions to spatiotemporal receptive-field structure and direction selectivity in simple cells of cat area 17. J Neurophysiol 81:1212–24.

Olveczky BP, Baccus SA, Meister M. 2003. Segregation of object and background motion in the retina. Nature 423:401–8.

Pasternak T, Schumer RA, Gizzi MS, Movshon JA. 1985. Abolition of visual cortical direction selectivity affects visual behavior in cats. Exp Brain Res 61:214–7.

Pettigrew JD. 1974. The effect of visual experience on the development of stimulus specificity by kitten cortical neurones. J Physiol 237:49–74.

Ratliff F, Riggs LA. 1950. Involuntary motions of the eye during monocular fixation. J Exp Psychol 40:687–701.

Riggs LA, Ratliff F. 1952. The effects of counteracting the normal movements of the eye. J Opt Soc Am 42:872–873.

Rucci M, Casile A. 2004. Decorrelation of neural activity during fixational instability: Possible implications for the refinement of V1 receptive fields. Vis Neurosci 21:725–38.

Rucci M, Casile A. 2005. Fixational instability and natural image statistics: Implications for early visual representations. Network 16:121–38.

Rucci M, Edelman GM, Wray J. 2000. Modeling LGN responses during free-viewing: A possible role of microscopic eye movements in the refinement of cortical orientation selectivity. J Neurosci 20:4708–20.

Rucci M, Iovin R, Poletti M, Santini F. 2007. Miniature eye movements enhance fine spatial detail. Nature 447:852–5.

Saul AB, Feidler JC. 2002. Development of response timing and direction selectivity in cat visual thalamus and cortex. J Neurosci 22:2945–55.

Saul AB, Humphrey AL. 1990. Spatial and temporal response properties of lagged and nonlagged cells in cat lateral geniculate nucleus. J Neurophysiol 64:206–24.

Saul AB, Humphrey AL. 1992. Evidence of input from lagged cells in the lateral geniculate nucleus to simple cells in cortical area 17 of the cat. J Neurophysiol 68:1190–208.

Sengpiel F, Kind PC. 2002. The role of activity in development of the visual system. Curr Biol 12:R818–26.

Sherman SM, Spear PD. 1982. Organization of visual pathways in normal and visually deprived cats. Physiol Rev 62:738–855.

Singer W, Rauschecker JP. 1982. Central core control of developmental plasticity in the kitten visual cortex: II. Electrical activation of mesencephalic and diencephalic projections. Exp Brain Res 47:223–33.

Snodderly DM, Kagan I, Gur M. 2001. Selective activation of visual cortex neurons by fixational eye movements: Implications for neural coding. Vis Neurosci 18:259–77.

Steinman RM, Haddad GM, Skavenski AA, Wyman D. 1973. Miniature eye movement. Science 181:810–9.

Stent GS. 1973. A physiological mechanism for Hebb's postulate of learning. Proc Natl Acad Sci USA 70:997–1001.

Stryker MP, Harris WA. 1986. Binocular impulse blockade prevents the formation of ocular dominance columns in cat visual cortex. J Neurosci 6:2117–33.

Suarez H, Koch C, Douglas R. 1995. Modeling direction selectivity of simple cells in striate visual cortex within the framework of the canonical microcircuit. J Neurosci 15:6700–19.

van Hateren JH, Ruderman DL. 1998. Independent component analysis of natural image sequences yields spatio-temporal filters similar to simple cells in primary visual cortex. Proc Biol Sci 265:2315–20.

Weliky M, Katz LC. 1997. Disruption of orientation tuning in visual cortex by artificially correlated neuronal activity. Nature 386:680–5.

Wimbauer S, Wenisch OG, Miller KD, van Hemmen JL. 1997a. Development of spatiotemporal receptive fields of simple cells: I. Model formulation. Biol Cybern 77:453–61.

Wimbauer S, Wenisch OG, van Hemmen JL, Miller KD. 1997b. Development of spatiotemporal receptive fields of simple cells: II. Simulation and analysis. Biol Cybern 77:463–77.

Winterson BJ, Robinson DA. 1975. Fixation by the alert but solitary cat. Vision Res 15:1349–52.

Yarbus AL. 1967. Eye Movements and Vision New York: Plenum Press.

Yuille AL, Kammen DM, Cohen DS. 1989. Quadrature and the development of orientation selective cortical cells by Hebb rules. Biol Cybern 61:183–94.

Appendix A: Analysis of Correlated Activity

This appendix explains the derivations of our approximations of the second-order statistics of thalamocortical activity under conditions of normal and stroboscopic rearing.

Normal Rearing

Visual input statistics. In the presence of small eye movements, the retinal stimulus $I_r(\boldsymbol{x}, t)$ can be approximated by means of a Taylor series:

$$\begin{aligned} I_r(\boldsymbol{x}, t) &\approx I_r(\boldsymbol{x}, 0) + \nabla I_r(\boldsymbol{x}, 0)^T \cdot \boldsymbol{\xi}(t) + \frac{1}{2}\boldsymbol{\xi}^T(t) \cdot H(I_r(\boldsymbol{x}, 0)) \cdot \boldsymbol{\xi}(t) \\ &= I_r(\boldsymbol{x}, 0) + \frac{\partial I_r(\boldsymbol{x}, 0)}{\partial_x}\xi_x(t) + \frac{\partial I_r(\boldsymbol{x}, 0)}{\partial y}\xi_y(t) \\ &\quad + \frac{1}{2}\frac{\partial^2 I_r(\boldsymbol{x}, 0)}{\partial x^2}\xi_x^2(t) + \frac{1}{2}\frac{\partial^2 I_r(\boldsymbol{x}, 0)}{\partial y^2}\xi_y^2(t) + \frac{\partial^2 I_r(\boldsymbol{x}, 0)}{\partial xy}\xi_x(t)\xi_y(t) \end{aligned} \tag{6}$$

where $\xi = [\xi_x(t), \xi_y(t)]$ represents the eye movement trajectory.

In the Fourier domain, Eq. 6 gives:

$$\begin{aligned} I_r(\boldsymbol{f}, u) &= I(\boldsymbol{f})\delta(u) + if_x I(\boldsymbol{f})\xi_x(u) + if_y I(\boldsymbol{f})\xi_y(u) \\ &\quad + \frac{1}{2} - f_x^2 I(\boldsymbol{f})\mathcal{F}\{\xi_x^2(t)\}\frac{1}{2} - f_y^2 I(\boldsymbol{f})\mathcal{F}\{\xi_y^2(t)\} - f_x f_y I(\boldsymbol{f})\mathcal{F}\{\xi_x(t)\xi_y(t)\} \end{aligned} \tag{7}$$

where $\mathcal{F}$ denotes the operation of Fourier transform, $I(\boldsymbol{f})$ denotes the Fourier transform of the static image being observed and $\boldsymbol{f} = (f_x, f_y)$ and u represent spatial and temporal frequencies, respectively.

Equation 7 enables estimation of the spectral density of the retinal stimulus, P_{II}, during fixational instability:

$$\begin{aligned} P_{II} &= \left\langle \left| I_r(\boldsymbol{f}, u) \right|^2 \right\rangle_{\mathcal{I},\xi} \\ &= \delta(u)\left\langle \left| I(\boldsymbol{f}) \right|^2 \right\rangle_{\mathcal{I}} \left(1 - |\boldsymbol{f}|^2 < \mathcal{F}\{\xi^2(t)\} >_{\xi}\right) + |\boldsymbol{f}|^2 \left\langle \left| I(\boldsymbol{f}) \right|^2 \right\rangle_{\mathcal{I}} \mathcal{R}_{\xi\xi}(u) \\ &= P_A(\boldsymbol{f})\delta(u) + |\boldsymbol{f}|^2 P_S(\boldsymbol{f})\mathcal{R}_{\xi\xi}(u) \end{aligned} \tag{8}$$

where, we discarded the terms with order higher than $|\boldsymbol{f}|^2$ and assumed fixational eye movements to possess similar but uncorrelated statistics on the two axes of motion ($R_{\xi_x\xi_x} = R_{\xi_y\xi_y} = R_{\xi\xi}$, and $R_{\xi_x\xi_y} = 0$) and to maintain on average the eye on the fixation point ($\langle \xi_x(t) \rangle_\xi = \langle \xi_y(t) \rangle_\xi = 0$). In this equation, $P_S(\boldsymbol{f}) = \langle |I(\boldsymbol{f})|^2 \rangle_{\mathcal{I}}$ represents the power spectrum of the external stimulus, and $P_A(\boldsymbol{f})$ is equal to $\langle P_S(\boldsymbol{f})(1 - |\boldsymbol{f}|^2 \langle \mathcal{F}\{\xi^2(t)\} \rangle_\xi)$.

Eq. 8 shows that, during fixational eye movements, the power spectrum of the retinal input can be divided into two terms. The term $P_A(\boldsymbol{f})\delta(u)$ is confined to the plane at zero temporal frequency and represents the power spectrum of the average luminance profile impinging onto the retina. The second term —$|\boldsymbol{f}|^2 P_S(\boldsymbol{f})R_{\xi\xi}(u)$ — is space-time separable and represents the power spectrum of the fluctuations of luminance around their average. The spatial spectral density of this latter term is equal to the power spectrum of the first derivative of natural images, and its temporal spectral density is the power spectrum of eye movements.

Correlated activity

As explained in the Methods, the correlation kernel of a V1 unit η, $\widehat{K}_\eta(\boldsymbol{x}, t)$, was evaluated by pooling together the spatiotemporal inputs from all the 1764 geniculate units in the model. Each input was weighted by the mean correlation between the response of the considered geniculate unit and the response of η. Under the simplifying assumption that, at any given eccentricity, the kernels of geniculate cells with opposite polarities differ only in their sign, $K_\alpha^{\mathrm{ON}}(\boldsymbol{x}, t) = -K_\alpha^{\mathrm{OFF}}(\boldsymbol{x}, t) = K_\alpha(\boldsymbol{x}, t)$, Eq. 3 can be rewritten in a more compact form by means of the convolution operator:

$$\begin{aligned}\widehat{K}_\eta(\boldsymbol{x}, t) &= \mathcal{R}_\eta^{\mathrm{NL}}(\boldsymbol{x}) \star K_\alpha^{NL}(-\boldsymbol{x}, t) + \mathcal{R}_\eta^{\mathrm{L}}(\boldsymbol{x}) \star K_\alpha^{L}(-\boldsymbol{x}, t) \\ &= \mathcal{R}_\eta^{\mathrm{NL}}(\boldsymbol{x}) \star S_\alpha(-\boldsymbol{x}) \cdot H_\alpha^{\mathrm{NL}}(t) + \mathcal{R}_\eta^{\mathrm{L}}(\boldsymbol{x}) \star S_\alpha(-\boldsymbol{x}) \cdot H_\alpha^{\mathrm{L}}(t)\end{aligned} \tag{9}$$

where $\mathcal{R}_\eta^{\mathrm{NL}}$ and $\mathcal{R}_\eta^{\mathrm{L}}$ represent the differences between the patterns of correlation established by η with ON and OFF geniculate units with the same dynamics d (non-lagged, NL, or lagged, L): $\mathcal{R}_\eta^{\mathrm{d}} = \mathcal{R}_\eta^{\mathrm{ON,d}}(\boldsymbol{x}) - \mathcal{R}_\eta^{\mathrm{OFF,d}}(\boldsymbol{x})$.

Since the responses of simple cells were modeled by means of the linear combination of two space-time separable kernels, K_η^0 and K_η^{90} (see Eq. 2), the correlation patterns $\mathcal{R}_\eta^{\mathrm{NL}}$ and $\mathcal{R}_\eta^{\mathrm{L}}$ can also be expressed as the sums of two terms:

$$\begin{cases}\mathcal{R}_\eta^{\mathrm{NL}}(\boldsymbol{x}, t) = \mathcal{R}_\eta^{0,\mathrm{NL}}(\boldsymbol{x}, t) + \lambda \mathcal{R}_\eta^{90,\mathrm{NL}}(\boldsymbol{x}, t) \\ \mathcal{R}_\eta^{\mathrm{L}}(\boldsymbol{x}, t) = \mathcal{R}_\eta^{0,\mathrm{L}}(\boldsymbol{x}, t) + \lambda \mathcal{R}_\eta^{90,\mathrm{L}}(\boldsymbol{x}, t)\end{cases} \tag{10}$$

where each term represents the pattern of correlation between the responses of the considered population of geniculate units and one of the two components in η's kernel (0 or 90).

In the absence of rectification ($\theta = -\infty$ in Eq. 1), each of the term on the right-hand side of Eq. 10 can be estimated in the frequency domain on the basis of the input spectrum:

$$\mathcal{R}_\eta^{\mathrm{c,d}}(\boldsymbol{f}, u) \propto K_\eta^{\mathrm{c}}(\boldsymbol{f}, u) \overline{K}_\alpha^{\mathrm{d}}(\boldsymbol{f}, u) P_{II} \tag{11}$$

where c indicates the considered component in the V1 kernel (0 or 90), d refers to the dynamics of the considered geniculate population (non-lagged, NL or lagged, L), and $K_\alpha(\boldsymbol{f}, u)$ and $K_\eta(\boldsymbol{f}, u)$ represent the Fourier transforms of the spatiotemporal kernels $K_\alpha(\boldsymbol{x}, t)$ and $K_\eta(\boldsymbol{x}, t)$, respectively.

Substitution of our approximation of the power spectrum of visual input (Eq. 8) yields:

$$\begin{cases}\mathcal{R}_\eta^{\mathrm{NL}}(\boldsymbol{f}) = \int_{-\infty}^{\infty} \mathcal{R}_\eta^{\mathrm{NL}}(\boldsymbol{f}, u)\mathrm{d}u = \gamma^{0,\mathrm{NL}} S_\eta^0(\boldsymbol{f}) \overline{S}_\alpha^{\mathrm{NL}}(\boldsymbol{f}) |\boldsymbol{f}|^2 P_S(\boldsymbol{f}) + \gamma^{90,\mathrm{NL}} S_\eta^{90}(\boldsymbol{f}) \overline{S}_\alpha^{\mathrm{NL}}(\boldsymbol{f}) |\boldsymbol{f}|^2 P_S(\boldsymbol{f}) \\ \mathcal{R}_\eta^{\mathrm{L}}(\boldsymbol{f}) = \int_{-\infty}^{\infty} \mathcal{R}_\eta^{\mathrm{L}}(\boldsymbol{f}, u)\mathrm{d}u = \gamma^{0,\mathrm{L}} S_\eta^0(\boldsymbol{f}) \overline{S}_\alpha^{\mathrm{L}}(\boldsymbol{f}) |\boldsymbol{f}|^2 P_S(\boldsymbol{f}) + \gamma^{90,\mathrm{L}} S_\eta^{90}(\boldsymbol{f}) \overline{S}_\alpha^{\mathrm{L}}(\boldsymbol{f}) |\boldsymbol{f}|^2 P_S(\boldsymbol{f})\end{cases} \tag{12}$$

where we have also considered that $H_\alpha^{\mathrm{NL}}(0) = H_\alpha^{\mathrm{L}}(0) = H_\eta(0) = 0$. The coefficients γ in Eqs. 12 are given by:

$$\begin{cases}\gamma^{0,\mathrm{NL}} = \int_{-\infty}^{\infty} H_\eta^0(u) \overline{H}_\alpha^{\mathrm{NL}}(u) \mathcal{R}_{\xi\xi}(u)\mathrm{d}u \\ \gamma^{0,\mathrm{L}} = \int_{-\infty}^{\infty} H_\eta^0(u) \overline{H}_\alpha^{\mathrm{L}}(u) \mathcal{R}_{\xi\xi}(u)\mathrm{d}u \\ \gamma^{90,\mathrm{NL}} = \int_{-\infty}^{\infty} H_\eta^{90}(u) \overline{H}_\alpha^{\mathrm{NL}}(u) \mathcal{R}_{\xi\xi}(u)\mathrm{d}u \\ \gamma^{90,\mathrm{L}} = \int_{-\infty}^{\infty} H_\eta^{90}(u) \overline{H}_\alpha^{\mathrm{L}}(u) \mathcal{R}_{\xi\xi}(u)\mathrm{d}u\end{cases} \tag{13}$$

The correlation kernels given by Eqs. 12 closely match the receptive fields of modeled V1 cells. Indeed, Eqs. 12 can be simplified by considering that (1) the term $|\boldsymbol{f}|^2\, P_S(\boldsymbol{f})$ is approximately constant during viewing of natural images; and (2) for geniculate and cortical units at the same visual eccentricity $\overline{S}_\alpha(\boldsymbol{f})S_\eta(\boldsymbol{f}) \approx S_\eta(\boldsymbol{f})$ (see Casile and Rucci, 2006). Therefore:

$$\begin{cases} \mathcal{R}_\eta^{\mathrm{NL}}(\boldsymbol{x}) \approx \gamma^{0,\mathrm{NL}} S_\eta^0(\boldsymbol{x}) + \lambda\gamma^{90,\mathrm{NL}} S_\eta^{90}(\boldsymbol{x}) \\ \mathcal{R}_\eta^{\mathrm{L}}(\boldsymbol{x}) \approx \gamma^{0,\mathrm{L}} S_\eta^0(\boldsymbol{x}) + \lambda\gamma^{90,\mathrm{L}} S_\eta^{90}(\boldsymbol{x}) \end{cases} \tag{14}$$

where we converted the expressions into the space-time domain by means of Inverse Fourier Transform.

Substitution of the characteristics of eye movements and cell kernels into Eqs. 13 yields: $\gamma^{0,\mathrm{NL}} \approx \gamma^{90,\mathrm{L}} \gg \gamma^{0,\mathrm{L}} \approx \gamma^{90,\mathrm{NL}}$. Thus, Eqs. 14 further simplifies into:

$$\begin{cases} \mathcal{R}_\eta^{\mathrm{NL}}(\boldsymbol{x}) \approx S_\eta^0(\boldsymbol{x}) \\ \mathcal{R}_\eta^{\mathrm{L}}(\boldsymbol{x}) \approx \lambda S_\eta^{90}(\boldsymbol{x}) \end{cases} \tag{15}$$

and, from Eq. 9:

$$\begin{aligned} \widehat{K}_\eta(\boldsymbol{x}, t) &= \mathcal{R}_\eta^{\mathrm{NL}}(\boldsymbol{x}) \star S_\alpha(\boldsymbol{x}) \cdot H_\alpha^{\mathrm{NL}}(t) + \lambda \mathcal{R}_\eta^{\mathrm{NL}}(\boldsymbol{x}) \star S_\alpha(\boldsymbol{x}) \cdot H_\alpha^{\mathrm{L}}(t) \\ &\approx S_\eta^0(\boldsymbol{x}) \star S_\alpha(\boldsymbol{x}) \cdot H_\alpha^{\mathrm{NL}}(t) + \lambda S_\eta^{90}(\boldsymbol{x}) \star S_\alpha(\boldsymbol{x}) \cdot H_\alpha^{\mathrm{L}}(t) \\ &\approx S_\eta^0(\boldsymbol{x}) \cdot H_\alpha^{\mathrm{NL}}(t) + \lambda S_\eta^{90}(\boldsymbol{x}) \cdot H_\alpha^{\mathrm{L}}(t) \\ &= S_\eta^0(\boldsymbol{x}) \cdot H_\eta^0(t) + \lambda S_\eta^{90}(\boldsymbol{x}) \cdot H_\eta^{90}(t) \end{aligned} \tag{16}$$

which is identical to the definition of K_η in Eq. 2. In agreement with this analysis, the analytical predictions given by Eqs. 12 were very similar to the results obtained from simulations of the full model, as illustrated in the top row of Fig. 11.

Stroboscopic Rearing

Visual input statistics. In the presence of stroboscopic illumination, the visual input to the model is:

$$I_r^{\mathrm{strobo}}(\boldsymbol{x}, t) = \left(\sum_{k=-\infty}^{\infty} I_r(\boldsymbol{x}, t)\delta(t - k\Delta_s) \right) \star p(t) \tag{17}$$

where $\Delta_s = 125$ ms is the interval between two successive flashes, $I_r(\boldsymbol{x}, t)$ is the visual input that would occur under normal illumination, and $p(t)$ models visual persistence.

For small-amplitude nystagmus, the term I_r can again be approximated by a truncated Taylor series, as in Eq. 6:

$$P_{II}^{\mathrm{strobo}}(\boldsymbol{f}, u) \approx P_A(\boldsymbol{f})S(u) + |\boldsymbol{f}|^2 P_S(\boldsymbol{f})Q(u) \tag{18}$$

where $S(u) = P(u)\sum_{k=-\infty}^{\infty} \delta(u - kf_s)$, $Q(u) = P(u)\sum_{k=-\infty}^{\infty} \mathcal{R}_{\xi\xi}(u - kf_s)$ and $f_s = \frac{1}{\Delta_s}$ is the stroboscopic frequency.

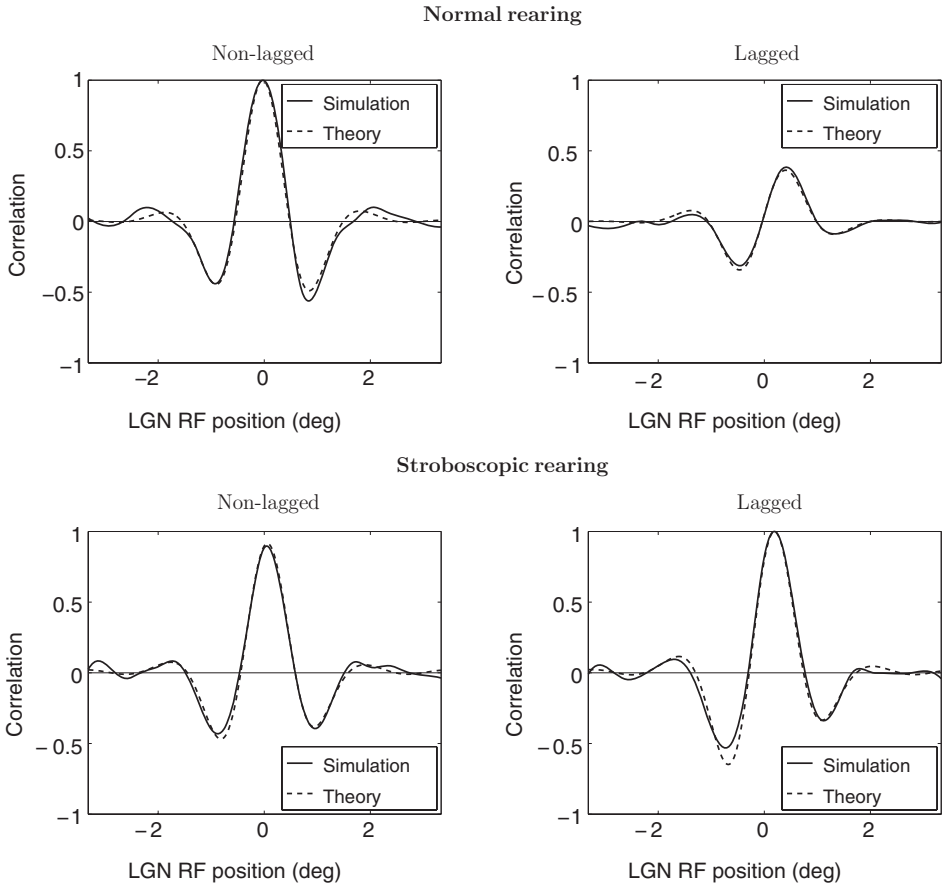

Figure 11. Comparison between the correlation kernels measured in simulations of the full model (solid line) and those given by the mathematical analysis of a linearized version of the model described in Appendix A (dashed line). Panels shows levels of correlation between Cell 1 in Fig. 2 and line arrays of non-lagged (*left*) and lagged LGN units (*right*) during normal (*top row*) and stroboscopic rearing (*bottom row*). The x-axis represents space relative to the center of the cortical receptive field. The similarity between analytical predictions and simulation results shown here for Cell 1 was also found for all the other V1 neurons in the model.

Equation 18 shows that, as in normal rearing, the power spectrum of visual input during fixation can be divided into the sum of two terms. The second term $|\boldsymbol{f}|^2 P_S(\boldsymbol{f})Q(u)$ represents the spectrum of the luminance fluctuations caused by the motion of the eye in the intervals between flashes. The spatial distribution of this term ($|\boldsymbol{f}|^2 P_S(\boldsymbol{f})$) is given by the spectral density of the first derivative of the stimulus; its temporal distribution ($Q(u)$) consists of replicas, at intervals u_s, of the spectrum of eye movements modulated by the function used to model retinal persistence. For simplicity, in this Appendix we assume perfect retinal persistence, *i.e.*, $p(t) = \mathrm{rect}(\frac{t-\Delta_s/2}{\Delta_s})$, so that $P(u) = \mathrm{sinc}^2(\frac{u}{u_s})$. With this assumption, the first term in Eq. 18 simplifies to $P_S(\boldsymbol{f})\delta(u)$ and represents the spectrum of the average luminance profile impinging onto the retina.

Correlated activity

For simplicity, we estimate correlated activity directly in the space/time domain rather than in the frequency domain. Eq. 10 remains valid under stroboscopic illumination, and each of the four correlation patterns is given by:

$$\begin{aligned}\mathcal{R}_{\eta}^{\mathrm{c,d}}(\boldsymbol{x}) &= \langle o_{\alpha}^{\mathrm{d}}(\boldsymbol{x}_1,t)\cdot o_{\eta}^{\mathrm{c}}(\boldsymbol{x}_2,t)\rangle_{\xi,\mathcal{I},t}\\ &= \langle S_{\alpha}(\boldsymbol{x}_1)H_{\alpha}^{\mathrm{d}}(t)\star I_r^{\mathrm{strobo}}(\boldsymbol{x}_1,t)\cdot S_{\eta}^{\mathrm{c}}(\boldsymbol{x}_2)H_{\eta}^{\mathrm{c}}(t)\star I_r^{\mathrm{strobo}}(\boldsymbol{x}_2,t)\rangle_{\xi,\mathcal{I},t}\end{aligned} \tag{19}$$

where o_{η}^{c} is the response of the considered component of η's kernel (0 or 90), o_{α}^{d} is the response of LGN unit α with dynamics d (non-lagged or lagged), and $\boldsymbol{x}=\boldsymbol{x}_1-\boldsymbol{x}_2$ is the distance between the centers of the two receptive fields.

Under assumptions on the statistics of eye movements similar to those of normal rearing, substitution of Eq. 17 into Eq. 19 yields two non-zero terms:

$$\begin{aligned}\mathcal{R}_{\eta}^{\mathrm{c,d}}(\boldsymbol{x}) &= \left\langle S_{\alpha}(\boldsymbol{x}_1)H_{\alpha}^{\mathrm{d}}(t)\star\frac{\partial I_r^{\mathrm{strobo}}(\boldsymbol{x}_1,t)}{\partial x}\cdot S_{\eta}^{\mathrm{c}}(\boldsymbol{x}_2)H_{\eta}^{\mathrm{c}}(t)\star\frac{\partial I_r^{\mathrm{strobo}}(\boldsymbol{x}_2,t)}{\partial x}\right\rangle_{\xi,\mathcal{I},t}\\ &+\left\langle S_{\alpha}^{\mathrm{d}}(\boldsymbol{x}_1)H_{\alpha}^{\mathrm{d}}(t)\star\frac{\partial I_r^{\mathrm{strobo}}(\boldsymbol{x}_1,t)}{\partial y}\cdot S_{\eta}^{\mathrm{c}}(\boldsymbol{x}_2)H_{\eta}^{\mathrm{c}}(t)\star\frac{\partial I_r^{\mathrm{strobo}}(\boldsymbol{x}_2,t)}{\partial y}\right\rangle_{\xi,\mathcal{I},t}\end{aligned} \tag{20}$$

The first term in Eq. 20 can be further expanded as:

$$\begin{aligned}&\left\langle S_{\alpha}(\boldsymbol{x}_1)\star\frac{\partial I_r(\boldsymbol{x}_1,0)}{\partial x}\cdot S_{\eta}^{\mathrm{c}}(\boldsymbol{x}_2)\star\frac{\partial I_r(\boldsymbol{x}_2,0)}{\partial x}\right\rangle_{\mathcal{I}}\\ &\cdot\left\langle H_{\alpha}^{\mathrm{d}}(t)\star\xi_x(t)\Delta(t)\star\mathrm{rect}\left(\frac{t-\Delta_s/2}{\Delta_s}\right)\cdot H_{\eta}^{\mathrm{c}}(t)\star\xi_x(t)\Delta(t)\star\mathrm{rect}\left(\frac{t-\Delta_s/2}{\Delta_s}\right)\right\rangle_{\xi,t}\\ &= S_{\alpha}(\boldsymbol{x})\star S_{\eta}^{\mathrm{c}}(-\boldsymbol{x})\star\left\langle\frac{\partial I_r(\boldsymbol{x},0)}{\partial x}\star\frac{\partial I_r(-\boldsymbol{x},0)}{\partial x}\right\rangle_{\mathcal{I}}\cdot\langle\overline{H}_{\alpha}^{\mathrm{d}}(t)\star\xi_x(t)\Delta(t)\cdot\overline{H}_{\eta}^{\mathrm{c}}(t)\star\xi_x(t)\Delta(t)\rangle_{\xi,t}\end{aligned} \tag{21}$$

where $\overline{H}_{\alpha}^{\mathrm{d}}(t)=H_{\alpha}^{\mathrm{d}}(t)\star\mathrm{rect}(\frac{t-\Delta_s/2}{\Delta_s})$ and $\overline{H}_{\eta}^{\mathrm{c}}(t)=H_{\eta}^{\mathrm{c}}(t)\star\mathrm{rect}(\frac{t-\Delta_s/2}{\Delta_s})$.

With some algebra, the term $\langle\overline{H}_{\alpha}^{\mathrm{d}}(t)\star\xi_x(t)\Delta(t)\cdot\overline{H}_{\eta}^{\mathrm{c}}(t)\star\xi_x(t)\Delta(t)\rangle_{\xi,t}$ in Eq. 21 can be expressed as:

$$\begin{aligned}&\left\langle\overline{H}_{\alpha}^{\mathrm{d}}(t)\star\xi_x(t)\Delta(t)\cdot\overline{H}_{\eta}^{\mathrm{c}}(t)\star\xi_x(t)\Delta(t)\right\rangle_{\xi,t}\\ &=\left\langle\sum_{k,j}\overline{H}_{\alpha}^{\mathrm{d}}(t-k\Delta_s)\overline{H}_{\eta}^{\mathrm{c}}(t-j\Delta_s)R_{\xi_x\xi_x}((j-k)\Delta_s)\right\rangle_t\end{aligned} \tag{22}$$

The right-hand side of Eq. 22 is periodic with period Δ_s. Thus, its time average is given by its integral over the period divided by the period length:

$$\begin{aligned}&\frac{1}{\Delta_s}\int_0^{\Delta_s}\sum_{k,j}\overline{H}_{\alpha}^{\mathrm{d}}(t-k\Delta_s)\overline{H}_{\eta}^{\mathrm{c}}(t-j\Delta_s)R_{\xi_x\xi_x}((j-k)\Delta_s)\mathrm{d}t\\ &=\frac{1}{\Delta_s}\sum_n\overline{H}_{\alpha}^{\mathrm{d}}(t)\star\overline{H}_{\eta}^{\mathrm{c}}(-t)\big|_{n\Delta_s}R_{\xi_x\xi_x}(n\Delta_s)\end{aligned} \tag{23}$$

where we have written the index j as $k+n$.

Using the same procedure also for the second term in Eq. 20, we obtain:

$$\mathcal{R}_{\eta}^{\mathrm{c,d}}(\boldsymbol{x}) \approx S_{\eta}^{\mathrm{c}}(\boldsymbol{x}) \cdot \frac{1}{\Delta_s} \sum_n \overline{H}_{\alpha}^{\mathrm{d}}(t) \star \overline{H}_{\eta}^{\mathrm{c}}(-t)\big|_{n\Delta_s} R_{\xi_x \xi_x}(n\Delta_s) \tag{24}$$

where we have considered presentation of natural images.

The average correlation patterns during stroboscopic rearing are obtained by substituting Eq. 24 into Eq. 10:

$$\begin{cases} \mathcal{R}_{\eta}^{\mathrm{NL}}(\boldsymbol{x}) = \gamma_{\mathrm{strobo}}^{0,\mathrm{NL}} S_{\eta}^{0}(\boldsymbol{x}) + \lambda \gamma_{\mathrm{strobo}}^{90,\mathrm{NL}} S_{\eta}^{90}(\boldsymbol{x}) \\ \mathcal{R}_{\eta}^{\mathrm{L}}(\boldsymbol{x}) = \gamma_{\mathrm{strobo}}^{0,\mathrm{L}} S_{\eta}^{0}(\boldsymbol{x}) + \lambda \gamma_{\mathrm{strobo}}^{90,\mathrm{L}} S_{\eta}^{90}(\boldsymbol{x}) \end{cases} \tag{25}$$

where:

$$\begin{cases} \gamma_{\mathrm{strobo}}^{0,\mathrm{NL}} & = \frac{1}{\Delta_s} \sum_n \overline{H}_{\alpha}^{\mathrm{NL}}(t) \star \overline{H}_{\eta}^{0}(-t)\big|_{n\Delta_s} R_{\xi\xi}(n\Delta_s) \\ \gamma_{\mathrm{strobo}}^{90,\mathrm{NL}} & = \frac{1}{\Delta_s} \sum_n \overline{H}_{\alpha}^{\mathrm{NL}}(t) \star \overline{H}_{\eta}^{90}(-t)\big|_{n\Delta_s} R_{\xi\xi}(n\Delta_s) \\ \gamma_{\mathrm{strobo}}^{0,\mathrm{L}} & = \frac{1}{\Delta_s} \sum_n \overline{H}_{\alpha}^{\mathrm{L}}(t) \star \overline{H}_{\eta}^{0}(-t)\big|_{n\Delta_s} R_{\xi\xi}(n\Delta_s) \\ \gamma_{\mathrm{strobo}}^{90,\mathrm{L}} & = \frac{1}{\Delta_s} \sum_n \overline{H}_{\alpha}^{\mathrm{L}}(t) \star \overline{H}_{\eta}^{90}(-t)\big|_{n\Delta_s} R_{\xi\xi}(n\Delta_s) \end{cases} \tag{26}$$

Substitution of the characteristics of nystagmus and cell kernels into Eqs. 26 yields $\gamma^{0,\mathrm{NL}} \approx \gamma^{90,\mathrm{NL}} \approx \gamma^{0,\mathrm{L}} \approx \frac{1}{2}\gamma^{90,\mathrm{L}}$, so that Eq. 25 simplifies into:

$$\begin{cases} \mathcal{R}_{\eta}^{\mathrm{NL}}(\boldsymbol{x}) \approx S_{\eta}^{0}(\boldsymbol{x}) + \lambda S_{\eta}^{90}(\boldsymbol{x}) \\ \mathcal{R}_{\eta}^{\mathrm{L}}(\boldsymbol{x}) \approx S_{\eta}^{0}(\boldsymbol{x}) + 2\lambda S_{\eta}^{90}(\boldsymbol{x}) \end{cases} \tag{27}$$

Equation 27 shows that, unlike the case of normal rearing, geniculate neurons with different timings exhibit correlated responses with both S_{η}^{0} and S_{η}^{90}. This pattern of correlated activity does not yield a spatial gradient of response timings, and correlation kernels do not exhibit direction selectivity. Fig. 11 shows that the correlation patterns predicted by Eq. 27 closely matched those measured in the simulations of stroboscopic rearing.

Appendix B: Modeling Synaptic Plasticity

In the *Results* section, we used correlation patterns to determine whether a V1 neuron would lose its initial degree of selectivity during the critical period. Correlation patterns indicate the direction in which development will evolve following eye opening, but do not enable prediction of the actual structure of receptive fields at the end of the critical period. This Appendix summarizes the results of additional simulations, in which we examined the maturation of cortical receptive fields when changes in synaptic connectivity were modeled explicitly.

In these simulations, four square arrays of 30 by 30 geniculate cells projected, through plastic synapses, to five cortical units. Each array contained neurons with similar polarity and dynamics, as in Fig. 1(b). The initial weight values of thalamocortical connections were set to replicate the five kernels shown in Fig. 2(a). Every cycle of the simulation consisted of the following three steps: (1) Sequential evaluation of the responses of LGN and V1 units; (2) computation of the patterns of

correlated activity; and (3) weight update according to a direct rule of Hebbian plasticity:

$$w_{i,j}^{\mathrm{p,d}}(n) = w_{i,j}^{\mathrm{p,d}}(n-1) + \kappa C_{i,j}^{\mathrm{p,d}}(n) \tag{28}$$

where n represents time in computational cycles. For each modeled cortical unit η, $w_{i,j}^{\mathrm{p,d}}$ in Eq. 28 represents the strength of the input from the geniculate unit with timing d (non-lagged or lagged) and polarity p (ON- or OFF-centered) at position (i, j) in the array, and $C_{i,j}^{\mathrm{p,d}}$ the corresponding level of correlation in the responses of pre- and post-synaptic units.

With this rule of synaptic plasticity, changes in neuronal connectivity are only driven by levels of correlation, so that weights can both increase and decrease. For simplicity, no limits were applied to the range of possible values assumed by synaptic weights, nor was a normalization mechanism included in the simulations. Thus, the results presented in this Appendix rely on the implicit assumption that plastic changes were restricted to an interval of finite duration, which models the

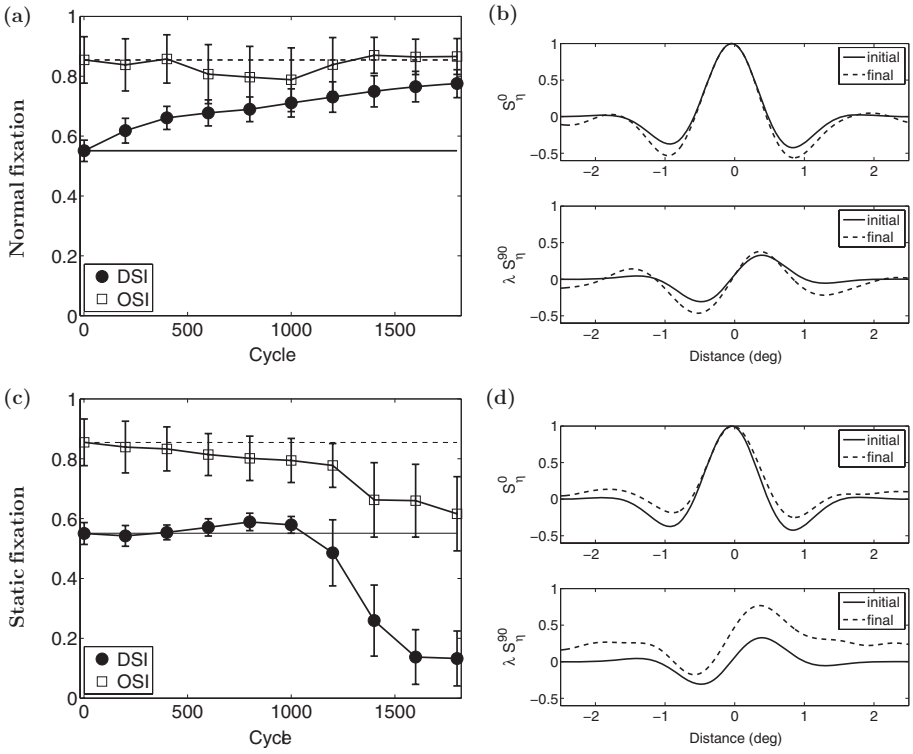

Figure 12. Results from simulations of synaptic plasticity. The two rows show results obtained when natural images were examined in the presence (*Normal Fixation*, top row) and in the absence of fixational eye movements (*Static Fixation* bottom row), respectively. (*a*, *c*) Temporal evolution of mean DSI and OSI ± s.e. measured across the five modeled cortical units. The two horizontal lines represent the mean DSI (solid line) and OSI (dashed line) at the time of eye opening. (*(b, d)*) Structure of the receptive field of Cell 1 in Fig. 2. The two panels in each figure show cross-sections of the two spatial components S_η^0 and λS_η^{90} in Eq. 2. Solid and dashed curves denote profiles measured at the beginning and at the end of the period of synaptic plasticity (see Appendix B for details).

critical period observed during development. According to Eq. 28, the speed of synaptic changes depends on both the scalar parameter κ and the strength of correlation. Connections from LGN units which are only moderately correlated with the considered V1 unit change their weights slowly, so that at the end of the critical period these synapses tend to be weak. In the simulations of Fig. 12, κ was set to 0.01, and the critical period was closed after $n = 1800$ iterations.

Fig. 12 shows the effect of exposing the model to an input signal that replicated the retinal stimulus during the normal instability of fixation. The visual input used in these simulations was identical to that of the simulations of Fig. 2. In agreement with the predictions derived from these previous simulations, both orientation and direction selectivity continued their normal refinement during exposure to natural stimulation. Fig. 12(b), shows the two spatial components S_η^0 and S_η^{90} of the receptive field of one of the modeled cortical units (Cell 1 in Fig. 2) both at the beginning and at the end of the simulations. These components were obtained by summing up the inputs from all geniculate units with the same temporal profile, each contribution weighted by the strength of the corresponding synapse. As shown by these data, Hebbian plasticity preserved and strengthened the regions with different polarities within the cell's receptive field. This enhancement in the segregation of thalamic afferents was responsible for the increment in the degree of direction selectivity reported in Fig. 12(a).

The refinement of response selectivity measured during exposure to normal retinal image motion contrasts with the developmental trajectory observed when the same images were examined statically. Both orientation and direction selectivity decreased in the absence of fixational instability. This effect originated from a corresponding loss in the spatial segregation of thalamic afferents. As shown in Fig. 12(c), cortical units now received input from geniculate neurons with different temporal and spatial characteristics located in the same region of visual space.

These results confirm the validity of our approach based on patterns of correlated activity. They clarify that spurious, accidental correlations have a minimal influence on development. Thalamic afferents which are strengthened at a particular fixation because of input peculiarities will be weakened at successive fixations. Only the afferents that match the spatial structure of the cortical receptive field are preserved and refined during learning.